UNIVERSIDADE DE LISBOA
FACULDADE DE CIÊNCIAS
DEPARTAMENTO DE QUÍMICA E BIOQUÍMICA

Biochemical characterization of a key cytochrome in respiratory electron transfer pathways from *Geobacter sulfurreducens*

Bruno Filipe Poeiras Mendes

Mestrado em Bioquímica
Bioquímica

Dissertação orientada por:
Prof. Doutor Carlos A. Salgueiro (orientador externo)
Prof. Doutor Cláudio M. Gomes (orientador interno)

2020

UNIVERSIDADE DE LISBOA
FACULDADE DE CIÊNCIAS
DEPARTAMENTO DE QUÍMICA E BIOQUÍMICA

Biochemical characterization of a key cytochrome in respiratory electron transfer pathways from *Geobacter sulfurreducens*

Bruno Filipe Poeiras Mendes

Mestrado em Bioquímica
Bioquímica

Dissertação orientada por:
Prof. Doutor Carlos A. Salgueiro (orientador externo)
Prof. Doutor Cláudio M. Gomes (orientador interno)

2020

“He who learns but does not think, is lost!
He who thinks but does not learn is in great danger.”
Confucius

AGRADECIMENTOS

Apesar de ser um documento apresentado em nome individual, esta tese resulta de um trabalho de equipa ao longo de um ano, durante o qual evoluí como pessoa, estudante e profissional. Envolveu a participação direta ou indireta de várias pessoas e só foi possível devido ao trabalho e dedicação de todas. Obrigado!

Agradeço ao Professor Doutor Carlos A. Salgueiro pela atenção, disponibilidade e paciência que demonstrou comigo durante a realização do trabalho e posteriormente na elaboração desta tese. Estou imensamente agradecido pela experiência adquirida, pela cedência de bibliografia e motivação para navegar pelo misterioso, vasto e interessante mundo da investigação. Também não poderia de deixar de agradecer o constante apoio e confiança depositada em mim para trabalhar consigo.

Agradeço ao Professor Doutor Cláudio M. Gomes pela disponibilidade e apoio na retificação desta dissertação para a obtenção do grau Mestre em Bioquímica. Obrigado pelos conhecimentos transmitidos.

Agradeço à Doutora Leonor Morgado a energia positiva, a preciosa ajuda, particularmente na fase inicial do trabalho de laboratório, e a insubstituível e inesquecível transmissão de saberes e conselhos acerca de uma vasta gama de assuntos.

Agradeço à Liliana Teixeira e à Marisa Ferreira, o vital apoio técnico, disponibilidade e companhia sempre que precisei. Aprendi, com ambas, inúmeras técnicas e aprofundei conhecimentos. Igualmente valiosa foi a ajuda no tratamento e discussão dos resultados. Foram as pessoas com quem passei mais tempo no laboratório. Fizeram-me rir e partilhámos discussões, frustrações e sucessos. Acima de tudo, estou grato por ter conhecido estas duas excelentes pessoas e profissionais, e por me terem ajudado o mais que podiam – especialmente nos dias em que o trabalho estava a correr menos bem. Obrigado por tudo.

Agradeço ao Tomás Fernandes e à Pilar Portela pela generosidade, preciosos conhecimentos, opiniões e acima de tudo pela igualmente insubstituível ajuda técnica e pessoal.

Nunca esquecerei os momentos de boa disposição passados ao longo do ano letivo anterior, dentro e fora do laboratório, com o professor e todos estes meus colegas. Desejo-vos o maior sucesso e tudo do melhor.

Agradeço também aos vários colegas e funcionários do Departamento de Química (não nomeio para que não falhe ninguém) que de diversas formas tornaram possível a realização do trabalho laboratorial (lavagem de material de laboratório, utilização de equipamentos, empréstimo de reagentes, ou outro tipo de apoios).

Aos meus pais, estarei eternamente grato por todo o amor, compreensão, apoio moral e financeiro que sempre me têm dado e por me permitirem ter chegado até aqui, apesar de todas as dificuldades. Ao meu pai, cujo apoio, ombro e conselhos, particularmente nos últimos meses, me ajudaram imenso quando eu mais precisava. À minha mãe Raquel, em especial, a quem devo a minha vida. Não tenho palavras que cheguem para descrever o imenso valor e importância de tudo o que tem feito por mim desde que nasci até agora. Tem estado presente e ouvindo-me sempre que precisei. Adoro-vos!

Um grande obrigado ao meu irmão Tiago pelo constante apoio e incentivo. Apesar de estar longe fisicamente, está todos os dias no meu pensamento e também sei que estou no dele. Abraço com saudades!

Por último, um agradecimento do fundo do meu coração à minha cara metade Alexandra, pelo amor verdadeiro e apoio incondicional. Todos os dias dá-me muita força, energia, coragem e paciência para mudar o que posso mudar e aceitar o que não posso mudar. Os obstáculos teriam sido certamente mais desmotivantes, difíceis de superar, e a conclusão teria sido muito menos saborosa e gratificante sem a mesma. Amo-teee!

RESUMO

As bactérias do género *Geobacter* têm um importante impacto no meio ambiente e potencial para aplicações biotecnológicas (biorremediação de contaminantes orgânicos e inorgânicos, produção de bioenergia e bioeletrónica). Estas bactérias conseguem transferir eletrões para aceitadores finais ou aceitá-los de elétrodos, um processo atualmente explorado na área da produção de bioenergia e eletrossíntese microbiana, respetivamente. Estas aplicações baseiam-se na troca eficiente de eletrões entre a célula e o exterior, processo designado por transferência extracelular de eletrões (TEE). No entanto, os mecanismos subjacentes à TEE ainda estão por compreender totalmente.

O principal objetivo desta Dissertação foi contribuir para a compreensão das vias TEE nas bactérias do género *Geobacter*. O trabalho focou-se na caracterização do citocromo GSU1740 recentemente identificado em *G. sulfurreducens*. Este citocromo é sobre-expresso durante a redução de fumarato em comparação com a redução de nitrato de Fe(III) apresentando também níveis significativos de expressão quando as células são crescidas na presença do aceitador final de eletrões de óxido de Fe(III) (insolúvel em água) comparativamente ao seu crescimento na presença de citrato de Fe(III) (solúvel em água) .

Neste trabalho foram optimizados os protocolos de expressão e de purificação do citocromo GSU140 o qual foi caracterizado através da utilização de técnicas biofísicas complementares, incluindo dicroísmo circular (DC), UV-visível, voltametria cíclica e ressonância magnética nuclear (RMN). A análise dos dados obtidos permitiu concluir acerca do tipo de estrutura secundária (dominada por hélices alfa), do número de grupos hemo (um), do seu estado de spin (baixo e alto no estado reduxido e oxidado, respectivamente) e respectiva coordenação axial (His-Met). Para além disso, foi também determinado o valor do potencial redox da proteína, na gama de pH 6 a 8, o qual cobre a franja - 66.8 a - 14.3 mV, relativamente ao electrodo padrão de hidrogénio.

Palavras-chave: *Geobacter sulfurreducens*, TEE, citocromo GSU1740, purificação, caracterizado, RMN, DC, UV-visível, voltametria cíclica.

ABSTRACT

Geobacter bacteria have an important impact on natural environments and potential for biotechnological applications (bioremediation of organic and inorganic contaminants, bioenergy production and bioelectronics). Geobacter cells can transfer towards extracellular terminal acceptors or accept electrons from electrodes, a process currently explored in bioenergy production and microbial electrosynthesis. These practical applications rely on an efficient transfer of electrons between the cell and its exterior, a process designated extracellular electron transfer (EET). However, the precise mechanisms underlying EET processes are still under debate.

The main objective of this Dissertation was contributing for the general understanding of the *Geobacter* bacteria EET pathways. The work focused on the preliminary characterization of newly identified GSU1740 cytochrome in *G. sulfurreducens*. This cytochrome is overexpressed during fumarate-reduction as compared to Fe(III)-citrate reduction and it was also found that cytochrome GSU1740 is significantly expressed in cells grown on Fe(III)-oxide (insoluble in water) compared with growth on the soluble electron acceptor Fe(III)-citrate (soluble in water).

In this work, several expression and purification protocols were optimized, for GSU1740 cytochrome, which was characterized using complementary biophysical techniques including circular dichroism, UV-visible absorption, cyclic voltammetry and nuclear magnetic resonance.

The analysis of the obtained data allowed for the conclusion about the type of secondary structure (dominated by alpha helices), the number of heme groups (one), its spin state (low and high in the reduced and oxidized state, respectively) and respective axial coordination (His-Met). In addition, the protein redox potential value was also determined, in the pH range 6 to 8, which covers from - 66.8 to - 14.3 mV, relative to the standard hydrogen electrode.

Keywords: *Geobacter sulfurreducens*, EET, GSU1740 cytochrome, purification, characterized, NMR, CD, UV-visible absorption, cyclic voltammetry.

TABLE OF CONTENTS

LIST OF FIGURES

LIST OF TABLES

ABBREVIATIONS, SYMBOLS AND CONSTANTS

1D	One dimensional
2xYT	2x Yeast extract-tryptone medium
AH_2QDS	Anthrahydroquinone-2,6-disulphonate
AMP	Ampicillin
AQDS	Anthraquinone-2,6-disulphonate
ATP	Adenosine triphosphate
bp	base-pair(s)
ccm	Cytochrome *c* maturation
CD	Circular dichroism
CLO	Chloramphenicol
CT	Charge-transfer
CV	Cyclic voltammetry
DNA	Deoxyribonucleic acid
dNTPs	Deoxynucleotides
DSS	4,4-dimethyl-4-silapentane-1-sulfonic acid
E. coli	*Escherichia coli*
EET	Extracellular electron transfer
EPR	Electron paramagnetic resonance
ESEEM	Electron-spin echo envelope modulation
ESI	Electrospray ionisation
FID	Free induction decay
G. sulfurreducens	*Geobacter sulfurreducens*
IEX	Ion exchange chromatography
IM	Inner membrane
IPTG	Isopropyl-β-D-1-thiogalactopyranoside
IUPAC	International Union of Pure and Applied Chemistry
kb	kilo base (1000 bp)
LB	*Luria-Bertani* médium
LBMS-IM	Laboratory for Biological Mass Spectrometry, Isabel Moura
MacA	Membrane associated cytochrome A
MALDI	Matrix-assisted laser desorption/ionisation
MALDI-TOF	Matrix-assisted laser desorption/ionisation - Time of Flight
MCD	Magnetic circular dichroism

MQ	Menaquinone
MS	Mass spectrometry
MW	Molecular-weight
MWCO	Molecular-weight cut-off
NADH	Nicotinamide adenine dinucleotide (reduced form)
NHE	Normal hydrogen electrode
NHE	Normal hydrogen electrode
NMR	Nuclear magnetic resonance
OD_{600nm}	Optical density at 600 nm
OM	Outer-membrane
Oma	Outer-membrane associated
Omb	Outer-membrane barrel
Omc	Outer-membrane cytochrome
PCR	Polymerase Chain Reaction
PDB	Protein Data Bank
Ppc	Periplasmic cytochrome
ppm	Parts per million
RF	Radiofrequency
RF	Restriction free
SDS	Sodium dodecyl sulfate
SDS-PAGE	Sodium dodecyl sulfate - polyacrylamide gel electrophoresis
SEC	Size-exclusion chromatography
TMBZ	Tetramethylbenzidine
TMS	Tetramethylsilane

ε	Molar extinction coefficient
I	Quantum spin number
γ	Gyromagnetic ratio
δ	Chemical-shift
$\vec{\mu}$	Magnetic moment of a nuclear spin
ν	Resonance frequency
E^0	Standard redox potential

AMINO ACID ABBREVIATIONS

Alanine	Ala	A
Arginine	Arg	R
Aspargine	Asn	N
Aspartate	Asp	D
Cysteine	Cys	C
Glutamate	Glu	E
Glutamine	Gln	Q
Glycine	Gly	G
Histidine	His	H
Isoleucine	Ile	I
Leucine	Leu	L
Lysine	Lys	K
Methionine	Met	M
Phenylalanine	Phe	F
Proline	Pro	P
Serine	Ser	S
Threonine	Thr	T
Tryptophan	Trp	W
Tyrosine	Tyr	Y
Valine	Val	V

1. INTRODUCTION

1.1. Dissimilatory metal reducing bacteria – an overview

Dissimilatory metal reduction is a common and fundamental process for the geochemistry of aquatic sediments, submerged soils, and terrestrial subsurface habitats, that occurs in the major groups of bacteria, by which they couple the oxidative metabolism of organic compounds with the reduction of extracellular metals [1,2]. Unlike other more frequent respiratory processes, where the final electron acceptor is a freely diffusible gas or a soluble molecule that can be reduced inside the cell, dissimilatory metal reducing bacteria (DMRB) are capable of sustaining their energy requirements by using extracellular metal ions [2].

DMRB have attracted significant attention because of the fact that their respiratory characteristics offer an important role in the environmental recycling and removal of metal contaminants from groundwater, predominantly Fe(III) [2]. Several of these microorganisms (*e.g. Desulfuromonas acetoxidans*, *Geobacter sulfurreducens*, *Geobacter metallireducens*, *Rhodoferax ferrireducens*, *Desulfobulbus propionicus*, *Enterococcus gallinarum*, *Shewanella putrefaciens* and *Shewanella oneidensis* [3]) belong to the group of exoelectrogens. These group of organisms can also couple the oxidative metabolism of organic compounds with the reduction of extracellular metals or electron transfer toward electrode surfaces from which electric current can be harvested in microbial fuel cells (MFC) [4,5]. *Geobacter* species in particular, are able to produce highly cohesive protein filaments with metallic-like conductivity, opening the possibility for design microbial-based electronic sensors and other devices [6].

Electron transfer towards extracellular terminal acceptors is one the most remarkable features of *Geobacter sulfurreducens* (*G. sulfurreducens*), which includes the reduction of insoluble toxic/radioactive metal and conversion of renewable biomass into electricity [7]. These capabilities opened a potential window for *Geobacter*-based applications in bioenergy production and bioremediation. Examples of such applications include degradation of hydrocarbon contaminants in soils, reduction of insoluble Fe(III) and Mn(IV) oxides, precipitation of uranium in contaminated aquifers and electron transfer to electrodes in microbial fuel cells from which electricity can be harvested. Given the broad range of biotechnological applications covered by *G. sulfurreducens* and other DMRB, it is essential to understand the functional mechanism of their respiratory pathways and the still unknown mechanisms that assist the extracellular electron transfer (EET). This would allow the scientific community to improve and optimize DMRB-based practical applications.

1.2. The bacterium *Geobacter sulfurreducens*

The family Geobacteraceae, where *G. sulfurreducens* is included, is part of the bacterial order Desulfuromonadales, which belongs to the subclass Deltaproteobacteria, in which all members are strictly anaerobic. [8].

Geobacter species are Gram-negative bacteria that play an important biogeochemical role in a diversity of natural environments. These species are mostly known for being DMRB, which can transfer electrons to insoluble metallic compounds in the environment and to the surface of terminal acceptors outside the cell to support their respiratory metabolism, in a process designated as extracellular electron

transfer (EET). This remarkable versatility permits *Geobacter* species to fill important niches in a variety of anaerobic environments [9]. These bacteria can also accept and donate electrons from electrodes, in current consuming biofilms, a process that is currently explored in microbial electrosynthesis systems.

Geobacter bacteria are abundant in diverse natural environments and show a remarkable respiratory versatility, since they are capable of sustaining their growth by using extracellular compounds, such as Fe(III), U(VI) or Mn(IV) oxides, as terminal electron acceptors, and can also utilize the most common soluble electron donors (*e.g.* acetate) and acceptors (*e.g.* fumarate). This includes the reduction of insoluble toxic/radioactive metal, which makes them important agents in several biogeochemical cycles, and the conversion of renewable biomass into electricity, by transferring electrons to electrode surfaces from which electricity can be harvested [2,7].

Geobacter bacteria were firstly considered as strict anaerobes that are naturally found in a variety of soils and sediments. But, when anaerobic dissimilatory metal reduction is stimulated by introducing organic electron donors into previously toxic subsurface sediments, *Geobacter* species rapidly become the predominant Fe(III)-reducing microorganisms in a variety of subsurface sediments, which suggests that there is a reservoir of *Geobacter* species in toxic aquifers [10].

The Gram-negative bacteria *G. sulfurreducens* are comma shaped rods and can be found in diverse natural environments, including contaminated soils and sediments where Fe(III) is an important respiratory terminal electron acceptor [7]. They can utilize acetate, lactate, formate, anthrahydroquinone-2,6-disulphonate (AH_2QDS) or hydrogen, as electron donors, and fumarate, sulphur, malate, Co(III), Cr(VI), Mn(IV) oxides, U(VI), Tc(VII), anthraquinone-2,6-disulphonate (AQDS), among others, as electron acceptors [7,11].

The important discoveries associated with *G. sulfurreducens* bacteria are summarized in Figure 1.1.

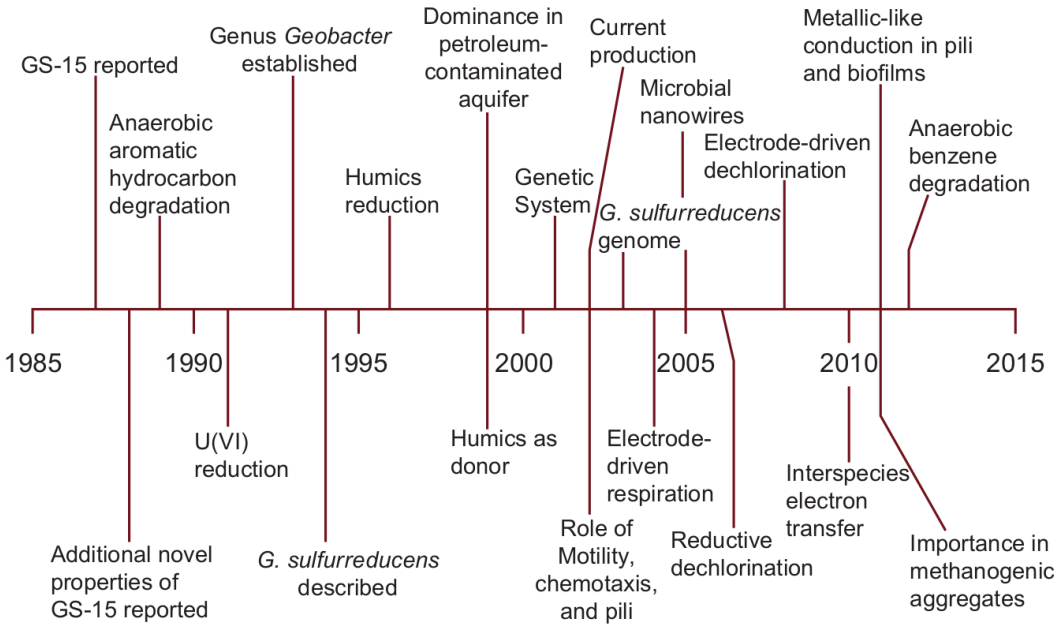

Figure 1.1. Timeline of important discoveries associated with *Geobacter* species. This figure was adapted from [7].

G. sulfurreducens was the first *Geobacter* species for which methods for genetic manipulation were developed and to have its genome fully sequenced and genetic systems established, and therefore it has

served as model organisms for functional genomic studies designed to understand *Geobacter* metabolism, gene regulation and EET [7,9]. G. *sulfurreducens* can tolerate exposure to oxygen for at least one day and readily grows with oxygen as the sole electron acceptor, at low concentrations (< 10 %). Additionally, the analysis of its genome revealed the presence of genes encoding typical enzymes for oxygen detoxification, such as catalase, cytochrome *c* oxidase or superoxide dismutase, which gives it the ability to tolerate exposure to high levels of oxygen. It is well documented that once oxygen is consumed in subsurface environments, *Geobacter* species can rapidly become the predominant Fe(III)-reducing microorganisms [10].

1.3. Extracellular electron transfer

Respiratory reduction of extracellular electron acceptors can be achieved by direct or indirect reduction of the acceptors [12,13]. Direct electron transfer is achieved via: the contact between redox proteins located on the bacteria surface of the cell; or electrically conductive appendages, also called biological nanowires (Fig. 1.2) [14]. Indirect reduction of acceptors can be mediated by: small redox-active molecules that are either secreted by the cell into the environment (endogenous electron shuttles) or are already available in the environment (exogenous electron shuttles); or bacterial-produced organic ligands, designated chelators, which solubilize metals prior to their reduction (see Fig. 1.2) [14].

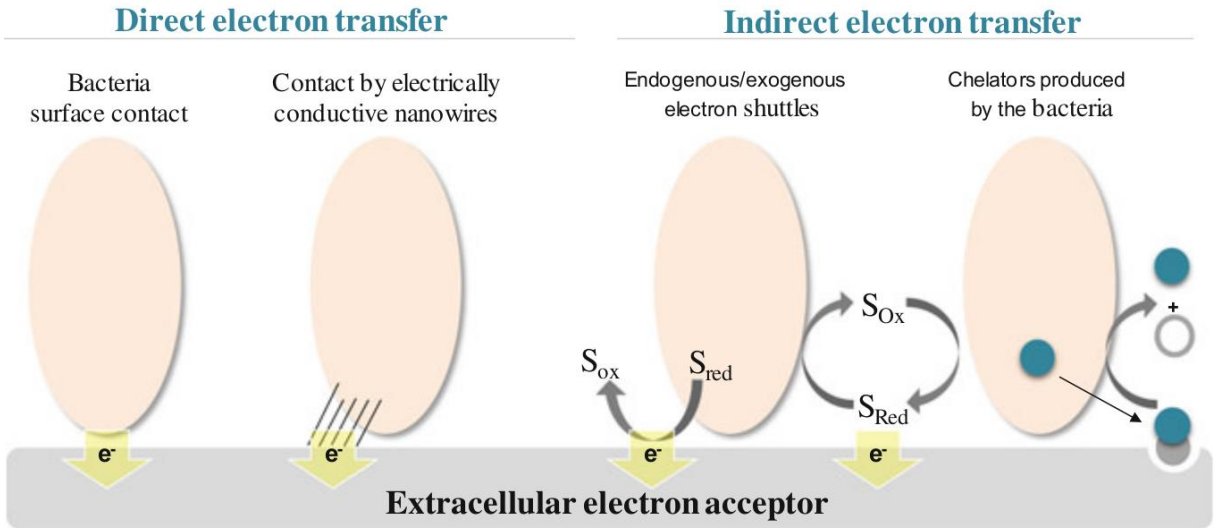

Figure 1.2. Schematic representation of the bacterial direct and indirect electron transfer mechanisms to the extracellular electron acceptors. S_{Ox} and S_{Red} correspond to oxidized and reduced electron shuttles, respectively. The action of chelator molecules is illustrated by circles: blue (chelator molecule); grey (insoluble acceptor); white (solubilized acceptor) [14]. This figure was adapted from [14].

1.3.1. Extracellular electron transfer pathways in *G. sulfurreducens*

The *G. sulfurreducens* PCA was described for the first time in 1994, after being isolated from surface sediments of a hydrocarbon-contaminated ditch near Norman, Oklahoma, USA [15]. This was the first bacterium described that couples the oxidation of acetate or hydrogen to the reduction of Fe(III). *G. sulfurreducens* has a versatile approach to capturing energy and carbon, having three enzyme systems capable of converting pyruvate to acetyl-CoA. These systems include a pyruvate-ferredoxin oxidoreductase and a pyruvate-formate lyase, both used by anaerobes, and a putative pyruvate dehydrogenase complex, largely found in aerobic organisms [16].

The analysis of the genome sequence of *G. sulfurreducens* revealed an unprecedented number of 111 putative *c*-type cytochromes, 73 of which are multiheme cytochromes (CXXCH, where X corresponds to any amino acid). The abundance of cytochromes and the co-existence of such a large number of multiheme cytochromes might help the organism to efficiently use a diverse range of respiratory pathways and highlights their involvement in a broad range of essential cellular functions and the importance of electron transport to this microorganism. This also suggests that *G. sulfurreducens* possesses electron transfer networks, with high flexibility and redundancy, allowing the reduction of diverse metal ions in natural environments [17]. In fact, several studies revealed a complex transcriptional response by these cells to different electron acceptors. Until now, no single gene deletion on the *G. sulfurreducens* genome was found to eliminate electron transfer to all electron acceptors, which confirms the complexity of the electron transfer networks in this bacterium [18-27].

Several studies have been performed in order to identify the cytochromes involved in the different reduction pathways used by *G. sulfurreducens*, and to elucidate their physiological roles. Proteomic analysis under different growth conditions and gene deletion studies were made, with special focus on *c*-type cytochromes since these proteins may play an important role in electron transfer to extracellular terminal acceptors. These *c*-type cytochromes are generally involved in electron transfer but can also have alternative physiological functions, such as transcriptional and post-transcriptional regulation [28, 29], and the deletion of individual genes for outer membrane *c*-type cytochromes did not significantly inhibit the ability of *G. sulfurreducens* to reduce humic substance or anthraquinone-2,6-disulfonate (AQDS, model compound for humics) and suggested that there are multiple routes for transfer of electrons to these acceptors [30].

Recent observations have led to the hypothesis that, depending upon the redox potential of the terminal electron acceptor, *G. sulfurreducens* utilizes different proteins and electron transfer pathways in the quinone pool regeneration [31,32]. At least five candidates for alternative quinone oxidoreductases exist in the *G. sulfurreducens* genome and two different routes were identified in response to the amount of energy available in a metal or electrode distant from the cell [32]. This is supported by several studies that revealed a complex transcriptional response by G. *sulfurreducens* to different electron acceptors [20,21,24]. The large number of *c*-type cytochromes [17] and the examination that no single deletion inhibits electron transfer to all electron acceptors serves as further confirmation of the complexity of the EET in *G. sulfurreducens* [18,19].

Many of the terminal electron acceptors that *G. sulfurreducens* can utilize are insoluble and, thus, unable to diffuse across the outer cell membrane to get into the cells. Consequently, reduction of these acceptors cannot occur in the periplasm, as for soluble acceptors, and requires electron transfer to the cell exterior [33, 34]. In order to assist this electron transfer across the outer cell membrane, the spatial disposition of the redox components in *G. sulfurreducens* cells differs from that of the majority of other microorganisms. The electron transfer proteins from this bacterium are strategically localized at the bacterial inner membrane (IM), periplasm or outer membrane (OM), allowing the transfer of electrons from intracellular carriers (*e.g.* NADH) to extracellular acceptors in a process termed extracellular electron transfer (EET) [23]. Previous proteomic studies revealed that 79 *c*-type cytochromes from *G. sulfurreducens* were expressed during growth on cultures containing Fe(III) citrate or Fe(III) oxide electron acceptors, using acetate as electron donor [20].

Considering this new perspective, *G. sulfurreducens* bacterium could also be used as a redox sensor to report the redox potential of an extracellular electron acceptor and represents an array of potential thermodynamic opportunities, where these bacteria rapidly adjust their respiratory strategy to adapt to changing conditions and take advantage of the available extracellular electron acceptor [35]. However, while numerous electron transfer proteins have been identified in *G. sulfurreducens*, the electron transfer pathways that allow this microorganism to obtain energy and the proteins implicated in each pathway are still far from being understood. It is consensual that NADH electrons are transferred to the quinone pool via an IM NADH dehydrogenase but from this point the electron transfer mechanisms toward the final electron acceptors are still under investigation. Obtaining a detailed characterization of cytochromes from *G. sulfurreducens* is essential before understanding these electron transfer mechanisms and delineate their physiological roles.

A better understanding of the microbial electrical energy production mechanisms can arise from the elucidation of the cellular strategies that allow chemical energy production from the reduction of natural extracellular terminal acceptors [36]. This is of major interest for the design of improved biotechnological applications (*e.g.* microbial fuel cell).

Other genetic studies identified cytochromes *c* OmcB, OmcS and OmcE, that are required for Fe(III) reduction in the outer membrane (OM) (see Fig. 1.3). MacA, PpcA, and OmcB are required for the reduction of soluble, chelated Fe(III) as well as poorly soluble Fe(III) oxide, whereas OmcS and OmcE are only required for Fe(III) oxide reduction. These results implied that these cytochromes might be part of an electron transport chain, moving electrons from the IM to the outer surface of the cell. However, recent studies have demonstrated that deleting some *c*-type cytochrome genes in *G. sulfurreducens* can have a negative impact on either the transcription or the translation of other cytochromes, suggesting that the impact of some gene deletions on Fe(III) reduction could be less direct than assumed previously [39].

The first studies envisioned that the inner-membrane-associated (IM-associated) diheme cytochrome MacA (GSU0466, the nomenclature of the genome is in accordance with www.genome.jp/kegg/genome.html) with 35 kDa molecular weight, might be involved in the electron transfer from the IM, through the periplasmic components of the EET network, to the outer surface of the cell [36, 37]. This cytochrome was also identified as a peroxidase and is also capable of exchanging electrons with the periplasmic *c*-type cytochrome PpcA [38]. Proteomic studies revealed that MacA is more abundant during growth with Fe(III) oxides *versus* Fe(III) citrate [20]. Gene knock-out studies implicated the deletion of *macA* gene in the inhibition of the expression of the *omcB* gene. Expression of the OM cytochrome OmcB in the *macA* gene deficient mutant restored the capability for Fe(III) reduction [39], and the similarity in expression patterns and mutant phenotypes between cytochromes MacA and OmcB suggests that they may function in the same or similar routes of electron transfer [19].

Initial studies also showed that *G. sulfurreducens* forms highly conductive pili when growing on Fe(III) oxides. It was shown that pili are required for electron transfer in order to reduce the Fe(III) oxides because these can serve as biological nanowires, working as the electrical connection between the cell and the surface of Fe(III) oxides [34]. Recent studies, however, revealed that the hexaheme cytochrome OmcS was localized along the pili (see Fig. 1.3) when *G. sulfurreducens* grows on Fe(III) oxides [40]. This suggests that pili may play a structural role by supporting *c*-type cytochromes along the way to the surface of iron oxides [41,42]. Additionally, it was proposed that abundant multiheme cytochromes, such as OmcS, can also play a role in electron storage in the absence of an electron acceptor [43], but the precise functions of these are not yet clarified and only a few respiratory chain components have been individually characterized.

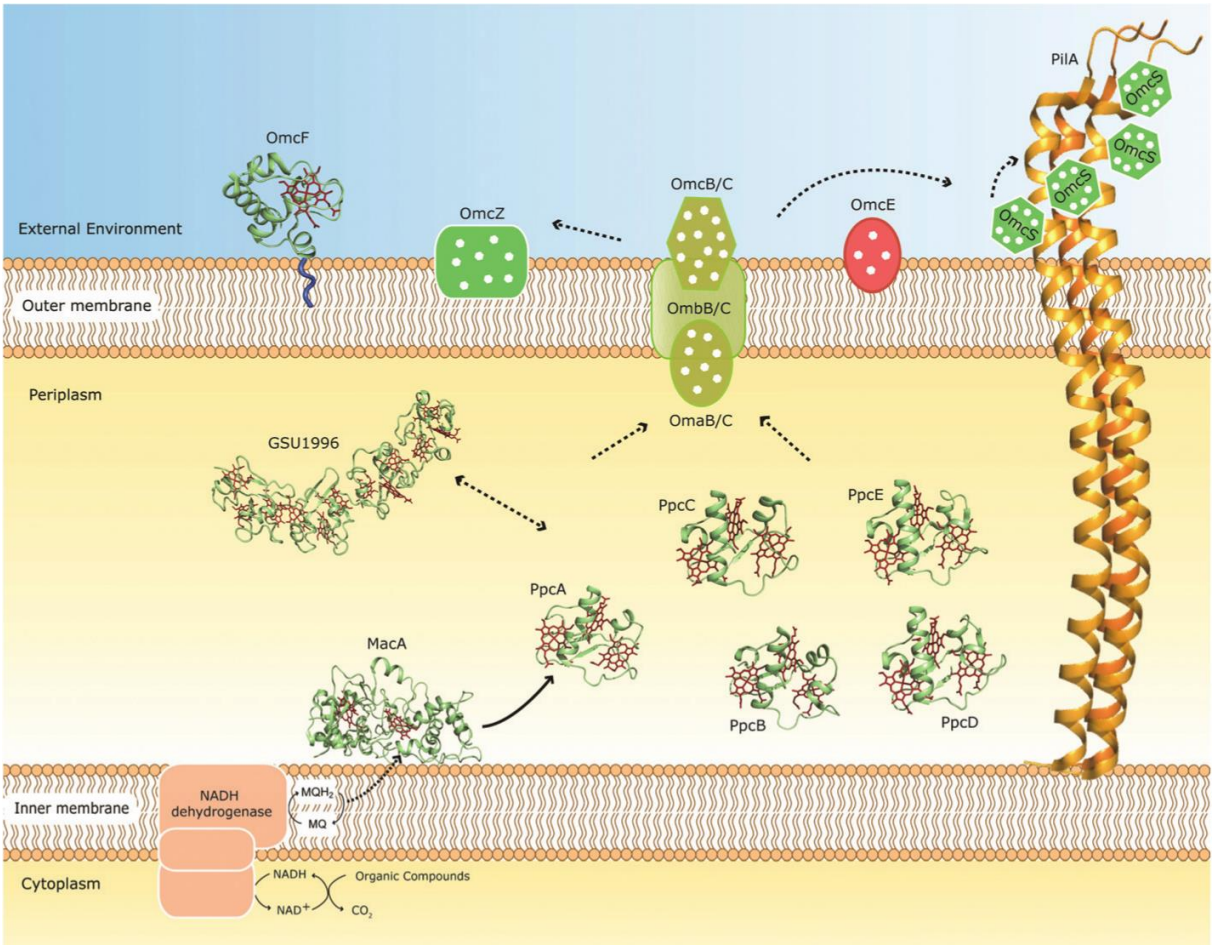

Figure 1.3. Proposed model for extracellular electron transfer in *G. sulfurreducens*. The oxidation of organic molecules releases electrons to the menaquinone (MQ) pool via NADH dehydrogenase. From this point, a network of *c*-type cytochromes is responsible for the electron transfer from the menaquiol (MQH_2) pool to the extracellular acceptor. MacA is proposed to accept electrons from the MQH_2 pool, which are delivered to multiheme periplasmic cytochromes, which then ensure electron transfer between cytoplasmic and OM electron transfer components. The arrows indicate the proposed flow for electrons. The structures of cytochromes from *G. sulfurreducens* were drawn using the PyMOL molecular graphics system: MacA (PDB 4AAL28); PpcA (PDB 2LDO30); PpcB (PDB 3BXU29); PpcC (PDB 3H3333); PpcD (PDB 3H4N33); PpcE (PDB 3H3433); GSU1996 (PDB 3OV032); OmcF (PDB 3CU437) and PilA (PDB 2M7G64). Cartoons illustrate electron transfer components for which no structures are available: (i) OM porin:cytochrome complexes OmaB/OmaC; OmbB/OmbC and OmcB/OmcC; (ii) cytochromes OmcZ, OmcE and OmcS; (iii) NADH dehydrogenase. The heme groups in OmcZ, OmaB/OmaC, OmcB/OmcC, OmcE and OmcS are represented by white circles. This figure was adapted from [9].

1.4. Cytochromes

Cytochromes are proteins containing one or more heme (iron–protoporphyrin IX) prosthetic groups and are involved in a wide range of biological functions, including simple electron transfer reactions, oxygen transport and storage via haemoglobin and myoglobin, oxygen reduction to the level of water by cytochrome oxidase, oxygenation of organic substrates, catalysis of peroxides, gas sensing and gene regulation [44-46]. The functional versatility of heme is mainly attributed to variables related with the type of heme groups and neighbour amino acids, with crucial factors including the ability of the protein environment to modulate heme reactivity, the number and nature of protein-donated axial ligands to iron, the extent of heme solvent exposure, the accessibility of the heme to exogenous ligands, the

distribution of polar and charged groups around the heme neighbourhood, and other specific properties of the heme-binding site in the protein [46].

These important proteins are among the most studied classes of biomolecules. Cytochromes are named accordingly to their heme type letter, in italic, and a number in subscript, depending on some intrinsic characteristics related to the protein axial ligands coordination, number of heme groups, optical or functional properties [47].

The type of heme groups is defined by the nature of substituents on the porphyrin macrocycle (see Fig. 1.4). The most common types of heme are heme *b* and heme *c*. Heme *b* is iron–protoporphyrin IX and binds noncovalently to the polypeptide chain of the protein, whereas heme *c* is characterized by the presence of two (rarely, one) covalent thioether bonds formed between sulfhydryl groups of two cysteine residues (Cys) and the heme vinyl groups at positions 2 and 4, in a conserved binding motif sequence CXXCH, where the X represents any amino acid. The stereochemistry of heme attachment is the same in all known examples of heme *c*. Other, less common, derivatives include heme *d1*, present in cytochrome *cd1* nitrite reductase, heme *a*, found in cytochrome c oxidase, and the related heme *o*, found in some bacterial oxidases [45, 46]. The heme group displays a central role in the functional modulation of these proteins and is constituted by four pyrrole subunits connected by methane bridges (protoporphyrin IX) and in the centre the iron ion is equatorially coordinated by four nitrogen atoms (Fig. 1.4b).

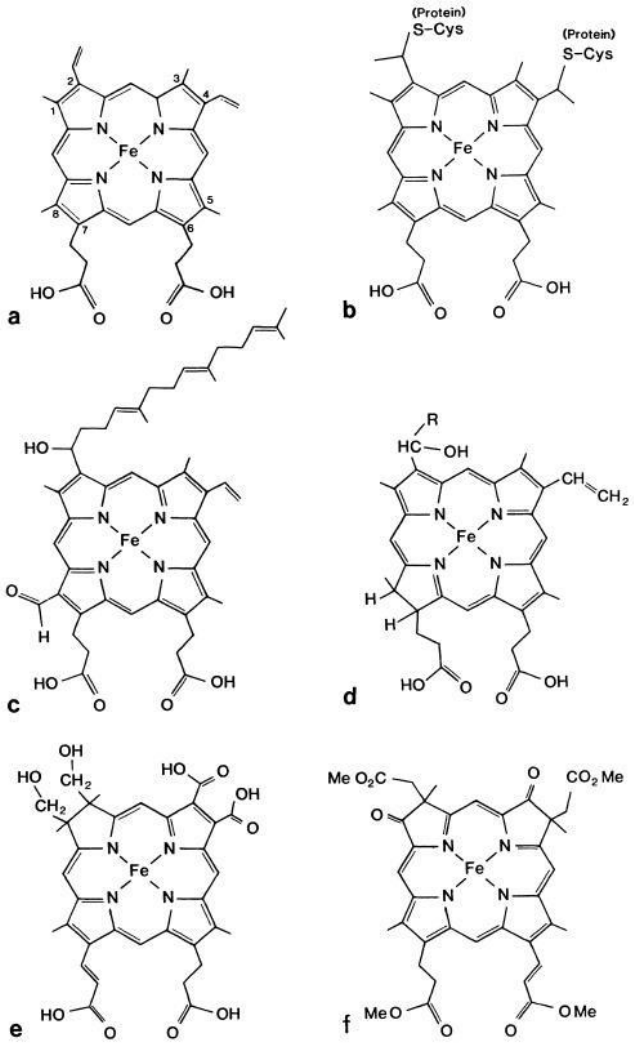

Figure 1.4. Different types of hemes found in cytochromes. The classification of the heme groups is based on the differences between the porphyrin molecules and types of polypeptide covalent attachments. a) *b*-type protoheme IX; b) *c*-type substituted protoheme IX; c) *a*-type, d) *d*-type; e) and f) d_1-type. This figure was adapted from [48].

1.5. Physicochemical features of *Geobacter*'s cytochromes *c*

Three-dimensional structures of biological macromolecules can be determined by X-ray crystallography and NMR at near atomic resolution. The structures obtained by NMR represent the average over oriented molecules in solution, whereas diffraction data represent an average over molecules arranged in a periodic crystal lattice. Despite their similarities and differences, X-ray crystallography and NMR are well established complementary high-resolution methods to analyse protein structure-function relationships.

The determination of monoheme and multiheme cytochromes structures is crucial to understand their functional mechanisms.

The Iron (0) is a transition metal with 26 electrons arranged in the electronic configuration $1s^2 2s^2 2p^6 3s^2 3p^6 3d^6 4s^2$, first numbers corresponds to the principal quantum number, the letters correspond to the orbital quantum number (s, p and d) and the superscripts correspond to the electron occupancies. This configuration is also represented as $[Ar]3d^6 4s^2$, to emphasize that the electron occupancies of the higher energy orbitals, 4s and 3d, superimposed on an argon core, determine the electronic properties and, ultimately, the chemical behaviour of the heme iron. Generally, in heme proteins, the iron exists in in two oxidation states: the ferrous state (Fe(II): $[Ar]3d^6 4s^0$) and the ferric state (Fe(III): $[Ar]3d^5 4s^0$). Iron(IV) ($[Ar]3d^4 4s^0$) is a less common state but often found in catalytic cycles of some enzymes, such as catalases or peroxidases [45].

In an iron atom there are five 3d-orbitals two orbitals of higher energy (d_{x2-y2} and d_{z2}, also known as the e_g set of orbitals) and three of lower energy (d_{xy}, d_{xz} and d_{yz}, also known as the t_{2g} set of orbitals). Each orbital holds a maximum of two electrons, and the distribution of electrons within these orbitals determines the electronic properties of iron. Besides, the electronic distribution of iron is influenced by the ligands coordinated to the iron ion [45]. There are two major energy terms that govern the distribution of electrons in the d-orbitals: the strength of the d-orbital splitting, which depends upon the electrostatic field created by the ligands and the energy required to pair electrons in the same orbital (pairing energy - P) [45].

The iron ion is in the high spin state if the d-orbital splitting is smaller than the pairing energy (weak crystal field) and therefore the electrons remain mostly unpaired in the orbitals (e_g and t_{2g}). Conversely, if the d-orbital splitting is larger compared to the pairing energy (strong crystal field), the electrons enter the t_{2g} orbitals and pair to produce the low spin state. Porphyrin is a strong ligand that places the iron ion close to a state where small energy differences between the axial ligand components of the field can cause the change of spin state [45]. Therefore, the determination of the spin state of a heme protein is important, because it provides information about the nature of the heme axial ligands and their stereochemistry. The heme spin state can be probed by a variety of spectroscopic techniques, including Electron Paramagnetic Resonance (EPR), Electron-spin Echo Envelope Modulation (ESEEM), Mössbauer, Magnetic Circular Dichroism (MCD) and Nuclear Magnetic Resonance (NMR).

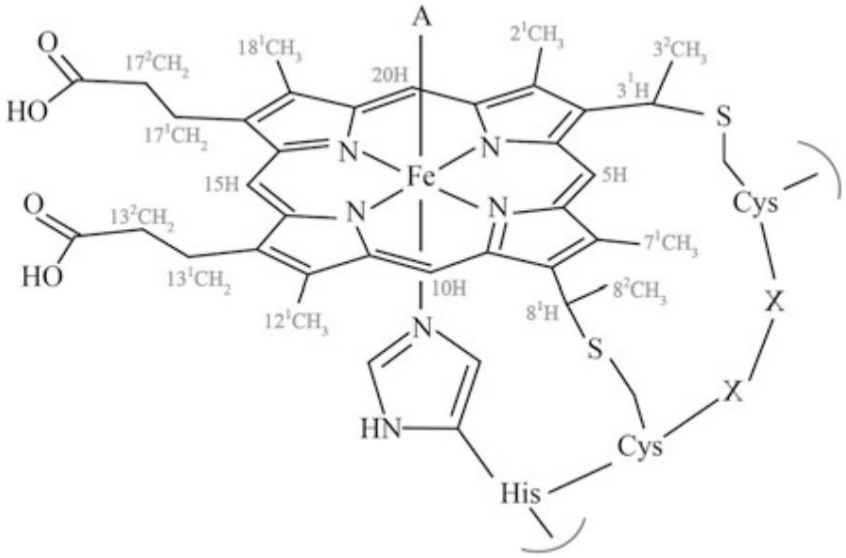

Figure 1.5. A *c*-type heme schematic representation and the correspondent polypeptide binding motif. The axial coordination position labelled with **A** can be free or occupied by the side chain of a methionine, histidine, asparagine or tyrosine residues and the IUPAC nomenclature for tetrapyrroles is illustrated in grey [14]. This figure was adapted from [14].

As depicted in Figure 1.5, four out the six heme iron coordination positions are equatorially occupied by pyrrole ring's nitrogen atoms. In most cases, one of the two axial coordination positions on the cytochromes *c* is occupied by the side chain of a histidine in the binding motif sequence, which is also designated as proximal ligand. The distal ligand is more variable and can be the side chain of a (i) methionine, which predominates in monoheme cytochromes *c*, (ii) histidine, particularly predominant in multiheme cytochromes *c* or (iii) asparagine, lysine or tyrosine, although with less frequency. In certain conditions, the distal position of the heme can also be transiently vacant, as observed for various cytochromes with enzymatic activity [14,47,49].

Therefore, in hemes *c* with histidine or methionine as distal ligands, the d-orbital splitting is larger than the pairing energy, meaning that these hemes will be in a low-spin state. In contrast, if the heme iron distal position is bond to the side chain of an asparagine, lysine, tyrosine or to a water molecule, the d-orbital splitting is smaller than the pairing energy, and the heme will be in a high-spin state. Heme proteins involved in electron transfer reactions usually have both axial positions occupied and hold histidine or methionine residues as distal ligands [14,45].

When the distal ligand is histidine or methionine residues, a strong crystal field and thus, a low spin state is observed. In contrast, if the side chain of asparagine, tyrosine or a water molecule bind the heme iron distal position, a high spin state will be observed [45]. Additionally, the identification of the iron axial coordination is important, because it determines the protein function, in most cases. Generally, the heme proteins involved in electron transfer reactions have both axial positions occupied and hold histidine or methionine residues as distal ligands. In the case of heme proteins with enzymatic activity that use a subtract molecule as heme axial ligand, an alternation between the iron penta- and hexa-coordinated forms is observed (*e.g.* peroxidases, catalases) [14,45].

1.5.1. Inner membrane cytochromes

Besides MacA, the main IM electron transfer components studied in the last few years have been CbcL (GSU0274) and ImcH (GSU3259) cytochromes. The CbcL protein contains a HydC/FdnI diheme *b*-type cytochrome linked to a 9-heme periplasmic cytochrome *c* domain [31]. On the other hand, the cytochrome ImcH was predicted to contain up to three transmembrane helices (depending on processing of a putative signal anchor), a region of NapC/NirT homology, and up to 7 heme *c*-type heme binding motifs [32].

1.5.2. Outer membrane cytochromes

The cytochrome OmcS has a molecular weight of 47 kDa, six heme groups and was purified from a strain that overproduces this protein. NMR together with UV-visible absorption spectroscopic studies allowed determining that all the heme groups are bis-histidinyl hexacoordinated and low spin in both fully oxidized and reduced states. The redox behaviour of OmcS was studied by redox titrations followed by UV-visible absorption. It was observed that the six redox centres are not equivalent and the redox curve spans over a large range of reduction potentials from -360 mV to -40 mV. The midpoint reduction potential at pH 7 was -212 mV. Reduced OmcS was able to transfer electrons in vitro to different substrates as Fe(III) and Mn(IV) oxides and humic substances [50].

OmcF is a monoheme cytochrome with sequence similarity to soluble c_6 cytochromes of photosynthetic algae and cyanobacteria. OmcF crystal structure was determined and was superimposable with a root mean square deviation (rmsd) of 1.1 Å to the structure of the cytochrome c_6 from the green alga *Monoraphidium braunii*. However, the function of these two proteins is probably different, since their biochemical properties are very distinct. OmcF has an isoelectric point (pI) of 7.8 while M. braunii cytochrome has a pI of 4.2, and their reduction potentials at pH 7 are +180 mV and +357 mV, respectively [51].

OmcZ was shown be present in two forms in *G. sulfurreducens*: a large one (OmcZL) and a small one (OmcZS) that is a cleaved product from the first. OmcZS is most probably the extracellular and active form. Redox titrations revealed that OmcZS functional working potential range is between -420 mV and -60 mV with a midpoint reduction potential of -220 mV. In vitro, OmcZS was able to transfer electrons to Fe(III) citrate, U(VI), Cr(VI), Au(III), Mn(IV) oxides, and AQDS, but not Fe(III) oxide [52].

1.5.3. Multiheme periplasmic cytochromes

In addition to the outer membrane cytochromes, an unusual periplasmic pool of five homologous triheme cytochromes (also known as c_7 cytochromes) was identified in *G. sulfurreducens* [53]. This family is considered essential in the bacterium electron transfer pathways since soluble periplasmic cytochromes are crucial for shuttling electrons from the cytoplasmic compartment to the outer membrane [36]. Multiheme cytochromes in the periplasm of Fe(III)-reducing bacteria (1, 2) and in sulfur- and sulfate-reducing bacteria (3-6) play critical roles in the environmental processing of many metals, including radionuclides.

The five triheme cytochromes are small proteins with approximately 10 kDa, 70 residues each and a pI of approximately 9, due to the high content in lysine residues. The most studied is the periplasmic cytochrome PpcA. PpcB, PpcC, PpcD, and PpcE (Gsc7) and share a 77 %, 62 %, 57 %, and 65 % amino acid sequence identity with PpcA, respectively. Due to the cellular location of these five cytochromes,

it was proposed that they are likely reservoirs of electrons, destined for the cell outer surface, bridging the electron transfer between the cytoplasm and the cell exterior [53].

The purified cytochrome c_7 PpcA is basic (pI 9.5) with 9.6 kDa that contains 71 residues and three covalently bound hemes and has an N-terminal amino acid sequence closely related to those of the previously described triheme *c* cytochromes of *Geobacter metallireducens* and *Desulfuromonas acetoxidans*. It is one of the smallest cytochrome *c*-type molecules with the highest ratio of hemes to amino acid residues. The purified protein can reduce Fe- (III), U(VI), Cr(VI), and other metal ions. The three-dimensional structure of PpcA from *G. sulfurreducens* has been determined by X-ray [53]. Studies suggest that PpcA serves as an intermediary electron carrier from acetate to terminal Fe(III) reductases in the outer membrane and is also involved in the transfer of electrons from acetate to U(VI) and humics [54].

1.7. Objectives and strategy

A new cytochrome, GSU1740, was found to be highly expressed during fumarate-reduction as compared to Fe(III)-citrate reduction [55]. Because the reduction of Fe(III) directly generates a source of Fe(II) for the cell, this suggests that when the environment is deficient in iron, shifts in the gene expression to favour of cytochromes with lower heme number may occur to accommodate iron scarcity. Also, it was also found that cytochrome GSU1740 is also significantly up-regulated in *G. sulfurreducens* cells grown on Fe(III)-oxide (insoluble in water) compared with growth on the soluble electron acceptor Fe(III)-citrate (soluble in water) [14]. Therefore, the present Dissertation is focused on the preliminary characterization of this newly identified *c*-type cytochrome.

Following the general introduction to *Geobacter* and cytochromes in the present Chapter. The optimization of the expression and purification protocols of the periplasmic cytochrome GSU1740 from *G. sulfurreducens*, as well as preliminary insights on the biochemical properties of the cytochrome are described in Chapters 2 and 3. The main conclusions and future perspectives are presented in Chapter 4.

1.8. References

[1] K.H. Nealson, D. Saffarini, Iron and Manganese in Anaerobic Respiration: Environmental Significance, Physiology, and Regulation, Annu. Rev. Microbiol., 48 (1994) 311–343.

[2] D.R. Lovley, Dissimilatory Metal Reduction, Annu. Rev. Microbiol., 47 (1993) 263–290.

[3] B. Erable, N.M. Duțeanu, M.M. Ghangrekar, C. Dumas, K. Scott, Application of electro-active biofilms, Biofouling, 26 (2010) 57–71.

[4] R. Kumar, L. Singh, Z.A. Wahid, M.F.Md. Din, Exoelectrogens in microbial fuel cells toward bioelectricity generation: a review, Int. J. Energy Res., 39 (2015) 1048–1067.

[5] B.E. Logan, B. Hamelers, R. Rozendal, U. Schröder, J. Keller, S. Freguia, P. Aelterman, W. Verstraete, K. Rabaey, Microbial Fuel Cells: Methodology and Technology, Environ. Sci. Technol., 40 (2006) 5181–5192.

[6] D.R. Lovley, Electromicrobiology, Annu. Rev. Microbiol., 66 (2012) 391–409.

[7] D.R. Lovley, T. Ueki, T. Zhang, N.S. Malvankar, P.M. Shrestha, K.A. Flanagan, M. Aklujkar, J.E. Butler, L. Giloteaux, A.-E. Rotaru, D.E. Holmes, A.E. Franks, R. Orellana, C. Risso, K.P. Nevin, *Geobacter*: The Microbe Electric's Physiology, Ecology, and Practical Applications, Adv. Microb. Physiol., 59 (2011) 1–100.

[8] E. Rosenberg, E.F. DeLong, S. Lory, E. Stackebrandt, F. Thompson (Eds.), The prokaryotes: Deltaproteobacteria and epsilonproteobacteria, Fourth edition, Springer-Verlag Berlin Heidelberg, 2014: pp. 45–73.

[9] T.C. Santos, M.A. Silva, L. Morgado, J.M. Dantas, C.A. Salgueiro, Diving into the redox properties of *Geobacter sulfurreducens* cytochromes: a model for extracellular electron transfer, Dalton Trans., 44 (2015) 9335–9344.

[10] W.C. Lin, M.V. Coppi, D.R. Lovley, *Geobacter sulfurreducens* Can Grow with Oxygen as a Terminal Electron Acceptor, Appl. Environ. Microbiol., 70 (2004) 2525–2528.

[11] A.M. Speers, G. Reguera, Electron Donors Supporting Growth and Electroactivity of *Geobacter sulfurreducens* Anode Biofilms, Appl. Environ. Microbiol., 78 (2012) 437–444.

[12] M. Breuer, K.M. Rosso, J. Blumberger, J.N. Butt, Multi-haem cytochromes in Shewanella oneidensis MR-1: structures, functions and opportunities, J. R. Soc. Interface, 12 (2015) 1–27.

[13] M.E. Hernandez, D.K. Newman, Extracellular electron transfer, Cell. Mol. Life Sci., 58 (2001) 1562–1571.

[14] C.A. Salgueiro, J.M. Dantas, Multiheme cytochromes, Springer-Verlag Berlin Heidelberg, 2016.

[15] F. Caccavo, D.J. Lonergan, D.R. Lovley, M. Davis, J.F. Stolz, M.J. McINERNEYl, *Geobacter sulfurreducens* sp. nov., a Hydrogen- and Acetate- Oxidizing Dissimilatory Metal-Reducing Microorganism, 60 (1994) 3752–3759.

[16] K.A. Jolley, D.G. Maddocks, S.L. Gyles, Z. Mullan, S.-L. Tang, M.L. Dyall-Smith, D.W. Hough, M.J. Danson, 2-Oxoacid dehydrogenase multienzyme complexes in the halophilic Archaea? Gene sequences and protein structural predictions, Microbiology, 146 (2000) 1061–1069.

[17] B.A. Methé, K. E. Nelson, J. A. Eisen, I. T. Paulsen, W. Nelson, J. F. Heidelberg, D. Wu, M. Wu, N. Ward, M. J. Beanan, R. J. Dodson, R. Madupu, L. M. Brinkac, S. C. Daugherty, R. T. DeBoy, A. S. Durkin, M. Gwinn, J. F. Kolonay, S. A. Sullivan, D. H. Haft, J. Selengut, T. M. Davidsen, N.

Zafar, O. White, B. Tran, C. Romero, H. A Forberger, J. Weidman, H. Khouri, T. V. Feldblyum, T. R. Utterback, S. E. Van Aken, D. R. Lovley, C. M. Fraser, Genome of *Geobacter sulfurreducens*: Metal Reduction in Subsurface Environments, Science, 302 (2003) 1967–1969.

[18] J.B. Rollefson, C.E. Levar, D.R. Bond, Identification of Genes Involved in Biofilm Formation and Respiration via Mini-Himar Transposon Mutagenesis of *Geobacter sulfurreducens*, J. Bacteriol., 191 (2009) 4207–4217.

[19] M. Aklujkar, M.V. Coppi, C. Leang, B.C. Kim, M.A. Chavan, L.A. Perpetua, L. Giloteaux, A. Liu, D.E. Holmes, Proteins involved in electron transfer to Fe(III) and Mn(IV) oxides by *Geobacter sulfurreducens* and *Geobacter uraniireducens*, Microbiology, 159 (2013) 515–535.

[20] Y.-H.R. Ding, K.K. Hixson, M.A. Aklujkar, M.S. Lipton, R.D. Smith, D.R. Lovley, T. Mester, Proteome of *Geobacter sulfurreducens* grown with Fe(III) oxide or Fe(III) citrate as the electron acceptor, Biochim. Biophys. Acta, 1784 (2008) 1935–1941.

[21] Y.-H.R. Ding, K.K. Hixson, C.S. Giometti, A. Stanley, A. Esteve-Núñez, T. Khare, S.L. Tollaksen, W. Zhu, J.N. Adkins, M.S. Lipton, R.D. Smith, T. Mester, D.R. Lovley, The proteome of dissimilatory metal-reducing microorganism *Geobacter sulfurreducens* under various growth conditions, Biochim. Biophys. Acta, 1764 (2006) 1198–1206.

[22] B.-C. Kim, B.L. Postier, R.J. DiDonato, S.K. Chaudhuri, K.P. Nevin, D.R. Lovley, Insights into genes involved in electricity generation in *Geobacter sulfurreducens* via whole genome microarray analysis of the OmcF-deficient mutant, Bioelectrochemistry, 73 (2008) 70–75.

[23] T. Mehta, M.V. Coppi, S.E. Childers, D.R. Lovley, Outer Membrane c-Type Cytochromes Required for Fe(III) and Mn(IV) Oxide Reduction in *Geobacter sulfurreducens*, Appl. Environ. Microbiol., 71 (2005) 8634–8641.

[24] K.P. Nevin, B.-C. Kim, R.H. Glaven, J.P. Johnson, T.L. Woodard, B.A. Methé, R.J. DiDonato, S.F. Covalla, A.E. Franks, A. Liu, D.R. Lovley, Anode Biofilm Transcriptomics Reveals Outer Surface Components Essential for High Density Current Production in *Geobacter sulfurreducens* Fuel Cells, PLoS ONE, 4 (2009) 1–11.

[25] R. Orellana, K.K. Hixson, S. Murphy, T. Mester, M.L. Sharma, M.S. Lipton, D.R. Lovley, Proteome of *Geobacter sulfurreducens* in the presence of U(VI), Microbiology, 160 (2014) 2607–2617.

[26] E.S. Shelobolina, M.V. Coppi, A.A. Korenevsky, L.N. DiDonato, S.A. Sullivan, H. Konishi, H. Xu, C. Leang, J.E. Butler, B.-C. Kim, D.R. Lovley, Importance of *c*-Type cytochromes for U(VI) reduction
by *Geobacter sulfurreducens*, BMC Microbiol., 7 (2007) 16.

[27] P.-L. Tremblay, Z.M. Summers, R.H. Glaven, K.P. Nevin, K. Zengler, C.L. Barrett, Y. Qiu, B.O. Palsson, D.R. Lovley, A *c*-type cytochrome and a transcriptional regulator responsible for enhanced extracellular electron transfer in *Geobacter sulfurreducens* revealed by adaptive evolution: Adaptive evolution and extracellular electron transfer, Environ. Microbiol., 13 (2011) 13–23.

[28] B.-C. Kim, C. Leang, Y.-H. R. Ding, R. H. Glaven, M. V. Coppi, and D. R. Lovley, OmcF, a Putative *c*-Type Monoheme Outer Membrane Cytochrome Required for the Expression of Other Outer Membrane Cytochromes in *Geobacter sulfurreducens*, J. Bacteriol., 187 (2005) 4505–4513.

[29] B.-C. Kim, X. Qian, C. Leang, M.V. Coppi, D.R. Lovley, Two Putative *c*-Type Multiheme Cytochromes Required for the Expression of OmcB, an Outer Membrane Protein Essential for Optimal Fe(III) Reduction in *Geobacter sulfurreducens*, J. Bacteriol., 188 (2006) 3138–3142.

[30] J.W. Voordeckers, B.-C. Kim, M. Izallalen, D.R. Lovley, Role of *Geobacter sulfurreducens* Outer Surface *c*-Type Cytochromes in Reduction of Soil Humic Acid and Anthraquinone-2,6-Disulfonate, Appl. Environ. Microbiol., 76 (2010) 2371–2375.

[31] L. Zacharoff, C.H. Chan, D.R. Bond, Reduction of low potential electron acceptors requires the CbcL inner membrane cytochrome of *Geobacter sulfurreducens*, Bioelectrochemistry, 107 (2016) 7–13.

[32] C.E. Levar, C.H. Chan, M.G. Mehta-Kolte, D.R. Bond, An Inner Membrane Cytochrome Required Only for Reduction of High Redox Potential Extracellular Electron Acceptors, mBio, 5 (2014) 1–14.

[33] K.A. Weber, L.A. Achenbach, J.D. Coates, Microorganisms pumping iron: anaerobic microbial iron oxidation and reduction, Nat. Rev. Microbiol., 4 (2006) 752–764.

[34] G. Reguera, K.D. McCarthy, T. Mehta, J.S. Nicoll, M.T. Tuominen, D.R. Lovley, Extracellular electron transfer via microbial nanowires, Nature, 435 (2005) 1098–1101.

[35] C.E. Levar, C.L. Hoffman, A.J. Dunshee, B.M. Toner, D.R. Bond, Redox potential as a master variable controlling pathways of metal reduction by *Geobacter sulfurreducens*, ISME J., 11 (2017) 741–752.

[36] D.R. Lovley, Bug juice: harvesting electricity with microorganisms, Nat. Rev. Microbiol., 4 (2006) 497–508.

[37] J.E. Butler, F. Kaufmann, M.V. Coppi, C. Nunez, D.R. Lovley, MacA, a Diheme *c*-Type Cytochrome Involved in Fe(III) Reduction by *Geobacter sulfurreducens*, J. Bacteriol., 186 (2004) 4042–4045.

[38] J. Seidel, M. Hoffmann, K.E. Ellis, A. Seidel, T. Spatzal, S. Gerhardt, S.J. Elliott, O. Einsle, MacA is a Second Cytochrome *c* Peroxidase of *Geobacter sulfurreducens*, Biochemistry, 51 (2012) 2747–2756.

[39] B.-C. Kim, D.R. Lovley, Investigation of direct vs indirect involvement of the *c*-type cytochrome MacA in Fe(III) reduction by *Geobacter sulfurreducens*, FEMS Microbiol. Lett., 286 (2008) 39–44.

[40] C. Leang, X. Qian, T. Mester, D.R. Lovley, Alignment of the *c*-Type Cytochrome OmcS along Pili of *Geobacter sulfurreducens*, Appl. Environ. Microbiol., 76 (2010) 4080–4084.

[41] D.R. Lovley, Extracellular electron transfer: wires, capacitors, iron lungs, and more, Geobiology, 6 (2008) 225–231.

[42] G. Reguera, R.B. Pollina, J.S. Nicoll, D.R. Lovley, Possible Nonconductive Role of *Geobacter sulfurreducens* Pilus Nanowires in Biofilm Formation, J. Bacteriol., 189 (2007) 2125–2127.

[43] A. Esteve-Núñez, J. Sosnik, P. Visconti and D. R. Lovley, Fluorescent properties of *c*-type cytochromes reveal their potential role as an extracytoplasmic electron sink in *Geobacter sulfurreducens*, Environ. Microbiol., 10 (2008) 497–505.

[44] F. Malatesta, G. Antonini, P. Sarti, M. Brunori, Structure and function of a molecular machine: cytochrome *c* oxidase, Biophys. Chem., 54 (1995) 1–33.

[45] G.R. Moore, G.W. Pettigrew, Cytochromes *c*: Evolutionary, Structural and Physicochemical Aspects, Springer-Verlag Berlin Heidelberg, 1990.

[46] S.E.J. Bowman, K.L. Bren, The chemistry and biochemistry of heme *c*: functional bases for covalent attachment, Nat. Prod. Rep., 25 (2008) 1118–1130.

[47] I. Bertini, G. Cavallaro, A. Rosato, Cytochrome *c*: Occurrence and Functions, Chem. Rev., 106 (2006) 90–115.

[48] G.W. Pettigrew, G.R. Moore, Cytochromes *c*: Biological Aspects, Springer-Verlag Berlin Heidelberg, 1987.

[49] L.J. Smith, A. Kahraman, J.M. Thornton, Heme proteins-Diversity in structural characteristics, function, and folding, Proteins Struct. Funct. Bioinforma., 78 (2010) 2349–2368.

[50] X. Qian, T. Mester, L. Morgado, T. Arakawa, M.L. Sharma, K. Inoue, C. Joseph, C.A. Salgueiro, M.J. Maroney, D.R. Lovley, Biochemical characterization of purified OmcS, a *c*-type cytochrome required for insoluble Fe(III) reduction in *Geobacter sulfurreducens*, Biochim. Biophys. Acta, 1807 (2011) 404–412.

[51] P.R. Pokkuluri, Y.Y. Londer, S.J. Wood, N.E.C. Duke, L. Morgado, C.A. Salgueiro, M. Schiffer, Outer membrane cytochrome *c*, OmcF, from *Geobacter sulfurreducens*: High structural similarity to an algal cytochrome c_6, Proteins Struct. Funct. Bioinforma., 74 (2009) 266–270.

[52] K. Inoue, X. Qian, L. Morgado, B.-C. Kim, T. Mester, M. Izallalen, C.A. Salgueiro, D.R. Lovley, Purification and Characterization of OmcZ, an Outer-Surface, Octaheme *c*-Type Cytochrome Essential for Optimal Current Production by *Geobacter sulfurreducens*, Appl. Environ. Microbiol., 76 (2010) 3999–4007.

[53] P.R. Pokkuluri, Y.Y. Londer, N.E.C. Duke, W.C. Long, M. Schiffer, Family of Cytochrome c_7-Type Proteins from *Geobacter sulfurreducens*: Structure of One Cytochrome c_7 at 1.45 Å Resolution, Biochemistry, 43 (2004) 849–859.

[54] J.R. Lloyd, C. Leang, A.L.H. Myerson, M.V. Coppi, S. Cuifo, B. Methe, S.J. Sandler, D.R. Lovley, Biochemical and genetic characterization of PpcA, a periplasmic *c*-type cytochrome in *Geobacter sulfurreducens*, Biochem. J., 369 (2003) 153–161.

[55] M. Embree, Y. Qiu, W. Shieu, H. Nagarajan, R. O'Neil, D. Lovley, K. Zengler, The Iron Stimulon and Fur Regulon of *Geobacter sulfurreducens* and Their Role in Energy Metabolism, Appl. Environ. Microbiol., 80 (2014) 2918–2927.

2. EXPERIMENTAL METHODS

2.1. Protein expression and purification

2.1.1. Expression vector

The expression vector containing the gene encoding for the protein GSU1740 was prepared by restriction free (RF) cloning method [1,2]. RF cloning is a polymerase chain reaction (PCR)-based method for design of DNA plasmids, also known as overlap extension PCR cloning) [1]. Compared to the conventional techniques the RF cloning method is more versatile. Indeed, conventional cloning techniques rely on enzymatic digestion of the insert and the vector before a clone can be obtained. This can cause problems because of the lack of suitable restriction sites or be hampered by the multiplicity of restriction sites in the DNA. On the other hand, RF cloning method simplifies the primer design, offers a less labour-intensive approach for making expression vectors and allows for the insertion of a sequence into any position within countless plasmids, independent of restriction enzyme recognition sites or homologous recombination sites within these sequences. For RF cloning the efficiency of obtaining positive clones is directly correlated to the effectiveness of the restriction digests [3]. The schematic representation of RF cloning is summarized in Figure 2.1.

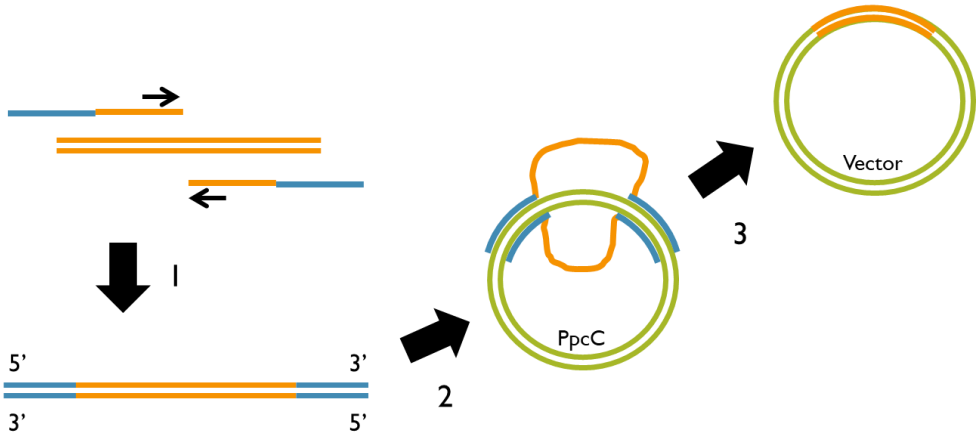

Figure 2.1. Schematic representation of restriction-free (RF) cloning. 1: PCR amplification of the targeted gene using previously designed primers. 2: PCR hybridization using a plasmid as a template. 3: Purification of the vector containing the cloned gene. Adapted from [3].

In this work, the mature DNA sequence of the gene encoding the protein GSU1740 was cloned using a pVA203-PpcC plasmid, a pUC derivative containing an ampicillin resistance gene, a *lac* promoter, which allows for the induction of transcription in the presence of isopropyl-β-D-1-thiogalactopyranoside (IPTG) (an analogous of lactose), and an *OmpA leader* sequence [4,5]. The primers were obtained with the Restriction Free Cloning web tool (rf-cloning.org) and contain a complementary sequence to both the desired gene and the target plasmid (Table 2.1).

Table 2.1. Sequences of DNA primers and inserted gene used for PCR hybridization (see Fig. 2.1). The melting temperatures (T_m) for each primer were calculated from the Thermo Scientific web tool (www.thermofisher.com) with the segment that hybridizes on the 5' site. The annealing temperature calculated for the pair of primers was 66 ºC, using the same tool. The sequences complementary to the pVA203-PpcC plasmid and to the inserted gene are highlighted in blue and in orange, respectively.

	DNA sequence	T_m (ºC)
Primer forward	5' GCTACCGTTGCGGCCGCCGCCGGGCAGGCGGAC 3'	65.5
Primer reverse	5' AGCTTGTCGACGGAGCTCGAATTTAGCCCCCGGGATTCCC 3'	63.2
Insert	5' GCCGGGCAGGCGGACAGGGGCAGAGAGCTTTTTGGAAGTACGC AACTGGGAACGAGCGGCAAAAGCTGCAGCAGCTGTCA TCCGGGCGGGAAGAAGCTCGAATGGGCCGGCTCCAGC TACGACGACGCGAAGCTTGCCGCCATCGTAAACCGTTG CATCGAAAAGGCCCTCAAGGGGAAACCGCTCGACCCG GGCGGAGAAGACATGAAGGCCCTTATGCAGCACATCA GGAGCTTTGGGAATCCCGGGGGCTAA 3'	-

The gene of interest was amplified by PCR, using the Phusion High-Fidelity DNA polymerase (Finnzymes). The composition of the PCR mix and cycling conditions are summarized in Tables 2.2 and 2.3, respectively. The PCR reaction volume was 50 µL to ensure the generation of enough megaprimer for the second PCR step. Negative control (see Table 2.2) were carried out for the PCR and the results were analysed by 1.5 % agarose gel electrophoresis, stained with GreenSafe Premium (NZYTech) (protocol presented in Appendix 2C). After this step, the PCR products were purified using the NZYMiniprep kit (NZYTech) and a Thermo Fischer Scientific™ NanoDrop™ was used to determine the concentration.

Table 2.2. Composition of the PCR solution used for the amplification of the gene encoding protein GSU1740 (reaction volume = 50 µL).

PCR reaction mix components	Final concentration		
	Amplification	Control 1	Control 2
PCR buffer	1x	1x	1x
Phusion High-Fidelity DNA polymerase*	1 U**	1 U**	1 U**
Deoxynucleotides (dNTPs)	0.20 mM	--	--
Primer forward	0.50 µM	0.50 µM	--
Primer reverse	0.50 µM	0.50 µM	--
DNA template (pGSU1740)	0.25 or 0.60 ng/µL	--	1.25 or 3.00 ng/µL

* The Phusion DNA polymerase, the Phusion GC/HF buffers and the dNTPs are all from Thermo Scientific.
**1 U = amount of enzyme necessary to catalyse the conversion of 1 µmole of substrate per minute.

Table 2.3. PCR cycling conditions used to amplify the gene encoding protein GSU1740. The annealing/extension time was calculated according to indication of 20 seconds/kb.

PCR step		T (ºC)	Time (seconds)
Initial denaturation		98	30
Denaturation	25x	98	7
Annealing		66	20
Extension		72	20
Final extension		72	600
Final hold		4	

The resulting double-stranded PCR product was purified and used as a set of mega-primers for a second PCR cycle. In this step, the pVA203-PpcC plasmid acted as a template, where each of the DNA strands annealed at a predesigned position and was extended in a linear-amplification reaction, in both directions. The mega-primers acted as long single-stranded overhangs that allow the two new DNA complementary strands of the plasmid to anneal, forming a double stranded nicked-plasmid (see Figure 2.1). The cycling conditions for the second PCR are given in the Tables 2.4 and 2.5.

Table 2.4. Composition of the solution used for the second PCR using the plasmid pVA203-PpcC as template (reaction volume = 20 μL).

PCR reaction mix components	Final concentration		
	Amplification	Control 1	Control 2
PCR buffer	1x	1x	1x
Phusion High-Fidelity DNA polymerase*	1 U**	1 U**	1 U**
Deoxynucleotides (dNTPs)	0.2 mM	--	--
GSU1740 insert	3.5 ng/μL	3.5 ng/μL	--
pVA203-PpcC vector	3.2 ng/μL	--	3.2 ng/μL

* The Phusion DNA polymerase, the Phusion GC/HF buffers and the dNTPs are all from Thermo Scientific.
**1 U = amount of enzyme necessary to catalyse the conversion of 1 μmole of substrate per minute.

Table 2.5. Cycling conditions used in the second PCR to obtain the expression vector. The annealing/extension time was calculated according to indication of 20 seconds/kb.

PCR step		T (ºC)	Time (seconds)
Initial denaturation		98	30
Denaturation	29x	98	7
Annealing		69	20
Extension		72	100
Final extension		72	600
Final hold		16	

As for the first PCR, negative controls (see Table 2.4) were carried out and the results were analysed by 1.5 % agarose gel electrophoresis, stained with GreenSafe Premium (NZYTech) (protocol and results presented in Appendix 2C). In order to eliminate the parental DNA templates (pVA203-PpcC) in solution, the PCR products were incubated with 0.4 µL of DpnI enzyme (NZYTech) for 120 minutes at 37 ºC. This reaction was conducted in the dark and then left for 20 minutes at 80 ºC for DpnI activation. The DpnI enzyme is specific for methylated and hemimethylated DNA, which are digested by the enzyme DpnI.

The newly synthesized plasmid containing the gene sequence for the protein mutant of interest, was then introduced into competent cells of *Escherichia coli* DH5α, where the DNA was sealed by endogenous enzymatic activity. First, a heat shock method was applied to create pores in the plasma membrane of the bacteria and allow for plasmid DNA to enter the bacterial cell. The solution containing the host and the expression vector was placed in ice for 30 minutes, followed by a period of 1 minute at 42 ºC and again a period of 1 minute in ice. Next, 400 µL of *Luria-Bertani* (LB) liquid medium (composition in Appendix 1) was added and the cells were incubated during 60 minutes, at 37 ºC and 200 rpm [1,6]. A control sample of competent cells with no added vector was prepared and subjected to the same procedures, in parallel.

Cells were then harvested by centrifugation at 4000 *xg* for 2 minutes. The pellet was resuspended in 100-200 µL of the supernatant and platted in LB solid medium (composition in Appendix 1) supplemented with 100 µg/mL ampicillin (AMP), for expression plasmid selection, and were left at 37 ºC overnight. Positive and negative controls were always carried out. The resulting colonies were screened by colony PCR [7] (with primers complementary to the pVA203-PpcC) and analysed by 1.3 % agarose gel electrophoresis.

Lastly, colonies with PCR products of the correct size were grown in 5mL LB liquid medium, supplemented with 100 µg/mL of AMP, at 37 ºC and 200 rpm. This was followed by plasmid extraction and purification, using the NZYMiniprep kit (NZYTech) and quantified using a Thermo Fischer Scientific™ NanoDrop™. The presence of the desired gene sequence was confirmed by DNA sequencing performed by STAB Vida. The plasmid containing the gene encoding for protein GSU1740 is hereafter designed by pVA203-GSU1740.

2.1.2. Heterologous expression

The main biochemical characteristics of cytochrome GSU1740 of concern for its expression and purification are curiously similar to those of all the PpcA-family cytochromes in terms of isoelectric point and molecular weight.

Table 2.6. Predicted biochemical characteristics of mature recombinant cytochrome GSU1740 expressed in *E. coli*. The presented molecular weight is approximated. The isoelectric point is theoretically predicted using the Compute pI/MW tool, from ExPASy Swiss Institute of Bioinformatics (https://www.expasy.org).

Isoelectric point	8.92
Molecular weight (Da)	9364
Residues	84
Amino acid sequence	AGQADRGRELFGSTQLGTSGKSCSSCHPGGKKLEWAGSSYDDA KLAAIVNRCIEKALKGKPLDPGGED**M**KAL**M**Q**H**IRSFGNPGG

1 µL of vector pVA203-GSU1740 (31.7 ng/µL) was added to 50 µL of *E. coli* containing plasmid pEC86 competent cells and then the same transformation method was applied, the only difference being that the cells were grown in 500 µL of 2x yeast extract - tryptone (2xYT) liquid medium (composition in Appendix 1). The pEC86 plasmid contains the gene which codes for the *c*-type cytochrome maturation (ccm) operon that allows *E. coli* to produce periplasmic cytochromes in aerobic conditions and a chloramphenicol (CLO) selection marker (NZYTech) [8,9].

Two cultures of transformed cells and two cultures of control cells were grown at 37 ºC overnight in 2xYT solid medium. For the transformed cells and the negative control, the medium was supplemented with 34 µg/mL of CLO (for pEC86 selection) and 100 µg/mL of AMP (for pVA203-GSU1740 selection), and for the positive control the medium was supplemented with only 34 µg/mL of CLO. Isolated colonies were used for growth in liquid media for protein overexpression.

2.1.2.1. *E. coli* strain selection

Six strains of *E. coli* containing plasmid pEC86 [BL21 (DE3), SF110, JM109, JCB7123, C43 (DE3), and Tuner (DE3)] were transformed with pVA203-GSU1740 plasmid and tested for heterologous expression of the GSU1740 protein. Transformed *E. coli* cells and the negative control cells were again incubated at 37 ºC overnight in 2xYT solid medium, containing 34 µg/mL of CLO and 100 µg/mL of AMP, and the positive control cells were again incubated at 37 ºC overnight in 2xYT solid medium containing only 34 µg/mL of CLO.

Colonies were obtained for four out of the six strains: BL21 (DE3), JM109, JCB7123 and Tuner (DE3). For each strain, one colony was transferred to two 250 mL erlenmeyers with 50 mL of 2xYT each and grown overnight at 30 ºC and 180 rpm. Protein expression was induced with 100 µM of IPTG from NZYTech when the OD_{600nm} reached the value of 0.7 or 1.5 followed by an overnight incubation at 30 ºC and 160 rpm.

A sample of cell culture was harvested each time: immediately before induction (uninduced sample); 2 hours after induction; and after the overnight incubation. The volume of the samples harvested was equivalent to 1 mL of cells at OD_{600nm} = 0.8, i.e., volume in mL = 0.8/OD_{600nm} of sample. The samples were all subjected to spin down at 4000 rcf for at least 2 minutes and the supernatant was carefully removed. The pellets were stored at -20 ºC.

The presence of the desired protein was confirmed by sodium dodecyl sulfate polyacrilamide gel electrophoresis (SDS-PAGE 15% acrylamide/bis-acrylamide) (protocol presented in Appendix 2) using a *Mini-PROTEAN® Electrophoresis System* (Bio-Rad), at 120 V. The molecular markers and samples containing loading buffer (composition in Appendix 1) were heated at 98 ºC for 5 minutes before being loaded onto the gel, to facilitate the protein denaturing process. Protein bands were stained with tetramethylbenzidine (TMBZ)/hydrogen peroxide (H_2O_2) to detect hemes or with BlueSafe (NZYTech) (protocols for both staining methods are presented in Appendix 2). The markers used were *Precision Plus Protein™ Dual Xtra Prestained Protein Standards* (Bio-Rad) with molecular weight range 2-250 kDa (Appendix 2A) and *PageRuler™ Unstained Low Range Protein Ladder* (Thermo Scientific) with a molecular weight range of 3.4-100 kDa (Appendix 2A).

2.1.2.2. Production of recombinant proteins

The *E. coli* strain showing higher levels of protein expression [BL21 (DE3)] were then used for large scale production. IPTG concentrations of 50 µM, 100 µM and 200 µM were tested first. A colony of this strain was transferred separately for two 250 mL erlenmeyers with 50 mL of 2xYT supplemented with

CLO and AMP, as previously described, and grown at 30 ºC and 180 rpm. Then, 1 % of these cell cultures were transferred to three erlenmeyer (2 L) containing 800 or 1000 mL of the same media, and aerobically grown at 30 ºC up to an OD_{600nm} of 0.7 at a shaking speed of 180 rpm. At this point, protein expression was induced with IPTG at a final concentration of 100 µM (the concentration that provided the best results). After induction, cells were left overnight, at 30 ºC and 160 rpm.

2.1.3. Protein purification

Cultures were harvested by centrifugation at 6400 *xg*, at 4 ºC, for 20 minutes. The cell pellet was gently resuspended in 30 mL of lysis buffer containing 15 mg of lysozyme (Fluka) per litre of initial cell culture (the detailed composition of the lysis buffer is given in Appendix 1). The cell suspension was incubated at room temperature for 15 minutes, then 30 mL of cold distilled water were added, followed by incubation on ice for 20 minutes with gentle shaking. The supernatant constituting the periplasmic fraction was recovered by centrifugation at 14000 *xg*, at 4 ºC, for 20 minutes. The periplasmic fraction was ultra-centrifugated at 44000 *xg*, at 4 ºC, for 60 minutes, to remove any precipitate, and the resultant pellets and supernatants analysed by SDS-PAGE (15 % acrylamide/bis-acrylamide) stained with TMBZ/H_2O_2 to detect hemes. After that, the supernatant was dialyzed twice against 10 mM Tris-HCl (pH 7.5) with a 3.5 kDa molecular-weight cut-off (MWCO) cellulose membrane (spectra/Pro), centrifugated at 8000 *xg*, at 4 ºC, for 30 minutes to remove cell debris. The supernatant obtained constituted the periplasmic faction.

The GSU1749 purification was achieved by combining a cation exchange and size exclusion chromatography steps. Cation exchange chromatography is a form of ion exchange chromatography (IEX), which is used to separate molecules based on their net surface charge. A protein's net surface charge changes with pH in respect of its isoelectric point (pI) value. At a pH equal to a protein's pI (8.92), the protein will carry no net charge. At a pH above the pI, the protein will carry a net negative surface charge. All the buffers used in this work had a pH below the protein's pI, which means that it carried a net positive surface charge [10]. So, the cation exchange chromatography used had a negatively charged resin with an affinity for molecules having net positive surface charges. The size-exclusion chromatography (SEC) used is a chromatographic method in which molecules in solution are separated on the basis of molecular hydrodynamic volume or size.

Several parameters and columns were tested before reaching an optimized protocol, which will be addressed in detail in the results and discussion section. In the cationic exchange step different columns were tested (*Econo-Pac Hitrap SP HP* cartridges (GE) and Bio-scale Mini UNOsphere S cartridges (Bio-Rad)) as well as elution flow rates, pH (6.5; 7.5 and 8.0) and gradient volume. In the gel filtration step flow rate was also optimized. The cation exchange chromatographic method was monitored with an *ÄKTA™ Pure Chromatography System* (GE Healthcare) and the size exclusion chromatography was monitored with an *ÄKTA™ Prime Plus Chromatography System* (GE Healthcare).

In the optimal purification the periplasmic fraction was loaded onto two 5 mL *Econo-Pac Hitrap SP HP* cartridges connected and equilibrated with 10 mM Tris-HCl pH 7.5 and eluted with a 20 column volume NaCl gradient (0-300 mM) at a flow rate of 0.7 mL/min. Brown-red coloured fractions of each peak were pooled together and concentrated to 1 mL in Amicon Ultra centrifugal filter units (Ultra-4, MWCO 3 kDa) and equilibrated with 100 mM sodium phosphate buffer pH 7.5, before being injected into a XK 16/70 column packed with *Superdex™ 75* (GE Healthcare) with a molecular weight range between 3 and 70 kDa. Protein was eluded at a flow rate of 0.5 mL/min. The protein purity was evaluated

by SDS-PAGE (15% acrylamide/bis-acrylamide), stained either for hemes (TMBZ staining) or with BlueSafe.

2.2. Molecular mass determination

Mass spectrometry (MS) is capable of the detailed study of extremely small quantities, down to a single molecule, of very large biological molecules. The mass spectrometers are composed of three basic components: ion source, mass analyser, and ion detector. MS requires a method to transfer molecules from solution or solid phase into the gaseous phase, because the measurements are carried out on ionised analytes. The two most commonly used ion sources are matrix-assisted laser desorption/ionisation (MALDI) and electrospray ionisation (ESI). After ionisation, the sample reaches the mass analyser, which separates ions by their mass-to-charge ratios (m/z). Ion motion in the mass analyser can be manipulated by electric or magnetic fields to direct ions to a detector, which registers the numbers of ions at each individual m/z value [11].

The experimental molecular-weight (MW) of the cytochrome was determined by mass spectrometry using a Ultraflex II MALDI-TOF Bruker-Daltonics spectrometer equipped with a LIFT cell and N_2 laser (Laboratory for Biological Mass Spectrometry, Isabel Moura). A matrix solution of sinapinic acid was in 70:30 water/acetonitrile with 0.07 % TFA. The mass spectrometer was operated with positive polarity in linear mode and spectra were acquired in the range of m/z 4000-18000. A total of 1000 spectra were acquired at each spot position at a laser frequency of 50 Hz. An external calibration with a protein calibration standard I from Bruker ($[M+H]^+$ of Insulin (5734.51m/z); Ubiquitin I (8565.76 m/z), Cytochrome C (12360.97 m/z), Myoglobin (16952.30 m/z); $[M+2H]^{2+}$ of cytochrome *c* (6180.99 m/z) and myoglobin (8476.65 m/z)) was used.

2.3. UV-visible absorption spectroscopy analysis

UV-visible absorption spectra were acquired at room temperature on a *Thermo scientific Evolution 201* spectrophotometer for the purified cytochrome in the oxidized and reduced states (10 mM Tris-HCl pH 7.5 at room temperature) using quartz cuvettes with 1 cm path length (Helma). Reduction of the samples was achieved with addition of sodium dithionite (Merck). The UV-visible absorption spectra of purified cytochrome GSU1740 was recorded in the range 200-750 nm, for both oxidized and reduced samples. The UV-visible absorption spectral features of the cytochrome were also used for protein quantification and identification of the heme spin state and heme axial ligands.

The molar extinction coefficient (ε) of purified cytochrome GSU1740 in the reduced form was determined for the α band at 552 nm. In order to attain this, the protein concentration was estimated by the Lowry method, using samples of horse-heart cytochrome *c* at known concentrations for the calibration curves. The absorptions were measured at 680 and 750 nm, which are the most reliable wavelengths for heme-containing proteins [12].

2.4. Nuclear Magnetic Resonance spectroscopy study

2.4.1. Fundamentals

Nuclear Magnetic Resonance (NMR) spectroscopy is a very powerful technique in the field of structural biology. This technique requires the existence of an external magnetic field and allows the study of the selective absorption of radiofrequency (RF) electromagnetic radiation by the nucleus. Nuclei are characterized by a quantum spin number (I), which can be determined from the atomic mass (number of protons and neutrons) and the atomic number (number of protons). When the atomic number and the atomic mass are even, nuclei have a quantum spin number of 0 (zero) (absence of magnetic properties, NMR silent nuclei). Then, when the atomic mass is odd (semi-integer quantum spin number) or when the atomic mass is even and the atomic number is odd (integer quantum spin number), nuclei have a quantum spin number different from zero and present magnetic properties (NMR active nuclei) [13].

The magnetic moment of a nuclear spin ($\vec{\mu}$) is proportional to its quantum spin number (I), by a gyromagnetic ratio, γ, as shown in Equation 1.1.

$$\vec{\mu} = \gamma I \tag{1.1}$$

The gyromagnetic ratio (γ) is a constant number and its magnitude depends on the type of nuclei and indicates the frequency at which they will precess in a fixed external magnetic field [13].

When no external magnetic field (B_0) is present, all nuclei of the same isotope have the same energy (degenerated states of energy). Once an external magnetic field is applied, a splitting of nuclei spin energies occurs. The energy of a state depends on the interaction of the aligned magnetic dipole with an externally applied magnetic field. At room temperature, the population difference between the two energy states is very small, on the order of 1 part in 10^6. This means that only a small fraction of the spins contributes to the signal intensity of the NMR spectrum, in other words the NMR spectroscopy is a relatively insensitive experimental technique because of the small excess of spins in the ground state. As a consequence, the use of stronger magnetic fields favours the NMR spectral resolution, since higher magnetic fields increase the population difference between the ground and excited NMR energy states, and the net absorption is dependent of this population difference [13].

When a nuclear transition between the two energy states occurs (resonance condition) an NMR signal is created. This transition will occur if the energy of the electromagnetic radiation applied is equal to the energy difference between the two states. Due to the effect of the electron density surrounding each individual proton, different Larmor frequencies will be detected for different protons, providing information about the nuclei and their interactions and/or surroundings. Thus, relative intensities of NMR signals reflect directly the number of nuclei contributing to the signals [13].

The frequency scale is represented in terms of a dimensionless number called chemical-shift (δ), which is related to the ratio between the resonance frequency of a certain nucleus in the sample (ν) and that of a reference standard (ν_{ref}), as shown in Equation 1.2 [12].

$$\delta = \nu - \nu_{ref} / \nu_{ref} \times 10^6 \tag{1.2}$$

TMS or DSS are normally used as references for the detected frequencies. By the equation above, the chosen references have a chemical shift of zero and the detected frequencies are expressed in ppm (parts per million). The NMR spectra, by convention, are plotted with chemical shift values increasing from the right to the left [12].

The simplest 1D experiment involves the application of a two building blocks (preparation and detection) pulse sequence. In the preparation, there is a delay time of relaxation that allows the magnetization to return to equilibrium. Next, a 90º radiofrequency pulse is applied during a certain time period (intrinsic of the sample), which rotates the equilibrium magnetization from the z-axis to the xy-plane. The recovery of the magnetization back to equilibrium is then detected in the form of a free induction decay (FID), during the detection period [12].

One dimensional (1D) spectra provides information about the preliminary stage of the sample in study, as well as foundations to design further experiments. In the paramagnetic oxidized state, the 1D ^{1}H-NMR spectra of high-spin cytochromes display extremely broad signals and some frequencies above 40 ppm (usually belonging to heme methyl substituents), while low-spin cytochromes present narrower spectral windows, with the main heme substituents frequencies ranging from 8 to 35 ppm. In the diamagnetic reduced state, 1D ^{1}H-NMR spectra for high-spin hemes present wider spectral regions (ranging from -15 up to 30 ppm) than low-spin ones (ranging from -5 up to 10 ppm). Thus, NMR can be explored to identify the spin-state of heme groups in proteins.

2.4.2. Sample preparation and experiment

All the NMR experiments were acquired in a Bruker Avance III 600 MHz spectrometer equipped with a triple-resonance cryoprobe (TCI) at 25 ºC and pH 7.01 (45 mM phosphate buffer, final ionic strength 100 mM prepared in 99% atom (CIL isotopes) $^{2}H_2O$). 1D-^{1}H NMR spectra were recorded for the GSU1740 in the oxidized state before and after the lyophilized to confirm its integrity. 1D-^{1}H NMR spectrum was also acquired for a reduced sample of GSU1740 prepared by the addition of sodium dithionite. The ^{1}H chemical shifts were calibrated using the water signal as internal reference. All the different spectra obtained were processed using TopSpin3.5.7^{TM} (Bruker BioSpin, Karlsruhe, Germany).

2.5. Circular Dichroism spectroscopy study

2.5.1. Fundamentals

Circular dichroism (CD) is an excellent method for rapidly evaluating the protein's secondary structure. Electromagnetic radiation is composed of two oscillating fields, magnetic and electric, perpendicular to each other. If the light is polarized by passing through suitable prisms or filters, its electric field will oscillate sinusoidally in a single plane [14]. The resulting polarised light can be viewed as being made of two circularly polarised components of equal magnitude, one rotating counter clockwise (left handed, L) and the other clockwise (right handed, R), that can be separated using a variety of prisms or electronic devices. CD refers to the differential absorption of these two components (see Fig. 2.4). If, after passage through the sample being examined, the L and R components are absorbed to different extents and also have different indices of refraction for the two waves, the resulting plane of the light wave is rotated and the light is said to be elliptically polarised (Fig. 2.4) [12,14].

A CD signal will be observed only when a chromophore is chiral (optically active), with absorption bands associated with a chiral centre or heme. Heme absorbance bands are CD-active because buckling

of the heme-plane gives rise to spiral electron motion. A CD spectrum is usually recorded as a plot against wavelength of the difference in absorbance between the L and R circularly polarised components ($\Delta A = A_L - A_R$). It is possible to determine, with a reasonable degree of accuracy, the secondary structure content of a protein by CD spectroscopy in the far-UV spectral region (190-260 nm) [12].

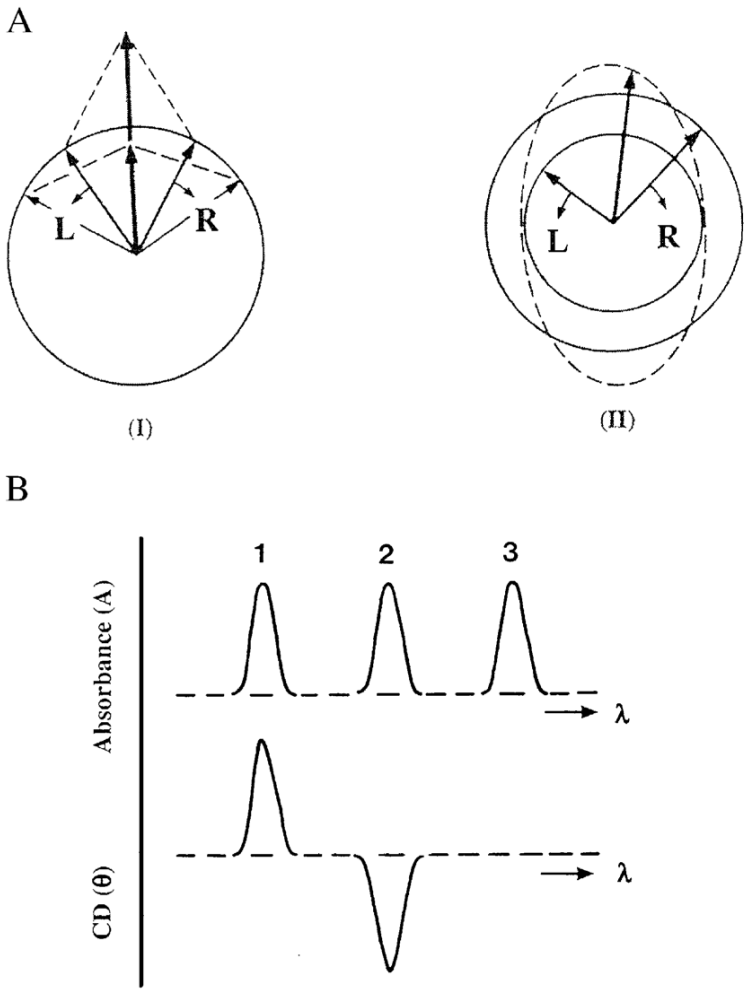

Figure 2.2. Origin of the CD effect. A: (I) the left (L) and the right (R) circularly polarised components of plane polarised light have the same amplitude and when combined generate plane polarised radiation; (II) the two components are of different magnitude and the resultant (dashed line) is elliptically polarised. B: The relationship between absorption and CD spectra. Band 1 has positive CD spectrum with L absorbed more than R; band 2 has a negative CD spectrum with R absorbed more than L; band 3 is due to an achiral chromophore [14]. This figure was adapted from [14].

2.5.2. Sample preparation and experiment

CD spectra of cytochrome GSU1740 (prepared in 45 mM NaPi at pH 7) were recorded at 25 ºC in the far-UV region, using a Chirascan qCD (BioLab) spectropolarimeter with a thermostatized cell support, using a 0.1 cm path-length cell quartz. The conformational stability of GSU1740 was monitored at 222 nm by thermal-induced denaturation, from 5 to 95 ºC, using a heating rate of 1.0 ºC/minute. The incubation at 95 ºC was followed by cooling back to 25 ºC and the recording of another far-UV CD spectra of cytochrome GSU1740, to observe if the thermal-induced denaturation was reversible.

2.6. Electrochemical studies

2.6.1. Fundamentals

Electrochemistry may be defined as the study of chemical reactions used to produce electric power or, alternatively, the use of electricity to affect chemical processes or systems [15]. Reactions that involve the transfer of electrons to and from molecules or ions are often referred to as reduction/oxidation (redox) reactions [16].

The reactions in all electroanalytical methods are heterogeneous in nature, as they take place at interfaces, usually electrode-solution boundaries, that differentiate otherwise identical solute molecules in those at a distance from the electrode and those close enough to participate in the redox reactions. Electrochemical responses or signals are divided in two main types: (i) faradaic or redox signals, which are caused by changes in the redox state of the analyte and that obey the Faraday Law and (ii) tensametric or “non-faradaic” signals, which are caused by changes in the differential capacitance of the electrode double layer due to the adsorption, desorption or reorientation of the sample on the electrode surface [16].

There are two main types of electrochemical methods to detect these signals, potentiometric and voltammetric [16]. Voltammetric (controlled potential) methods measure the changes in current of the sample, depending on the applied potential (against the potential of the reference electrode) at the working electrode. Potentiometric (controlled-current) methods are based on the application of a current on the working electrode, while measuring the difference of potential of the sample over time, to give an assessment of the composition of the sample [17].

Cyclic voltammetry (CV) is a basic voltammetric method extensively used for approaching qualitative information about electrochemical reactions (thermodynamics of redox processes, kinetics of heterogeneous electron transfer reactions, coupled chemical reactions or adsorption processes). CV consists of scanning linearly the potential of a stationary working electrode, using a triangular potential waveform (Fig. 2.2), and has the capability for rapidly observing redox behaviour over the entire potential range available [16].

During the potential sweep, the potentiostat measures the current resulting from the applied potential. The resulting current-potential plot is termed a cyclic voltammogram, which is a complicated time-dependent function of a large number of physical and chemical parameters [16]. The expected response of a reversible redox couple, during a single potential cycle is illustrated in Figure 2.3, assuming that only the oxidized form “O” is initially present. Thus, a negative-going potential scan is chosen for the first half-cycle, starting from a value where no reduction occurs [13].

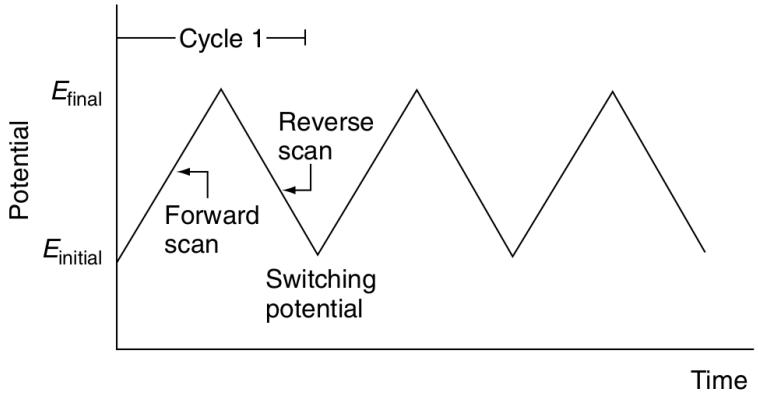

Figure 2.3. Potential–time excitation signal in a cyclic voltammetric experiment. Depending on the information sought, single or multiple cycles can be used. Each cycle is always composed of a forward scan and a reverse scan, where reduction and oxidation reactions occur, respectively [16]. The figure was adapted from [16].

A cathodic current begins to increase as the applied potential approaches the characteristic standard potential, E^0, for the redox process, resulting in a peak. Having crossed the potential region, where the reduction process takes place, the potential sweep direction is reversed. Throughout the reverse scan, reduced "R" species (generated in the forward half-cycle and accumulated near the surface) are re-oxidized back to "O", until it reaches an anodic peak.

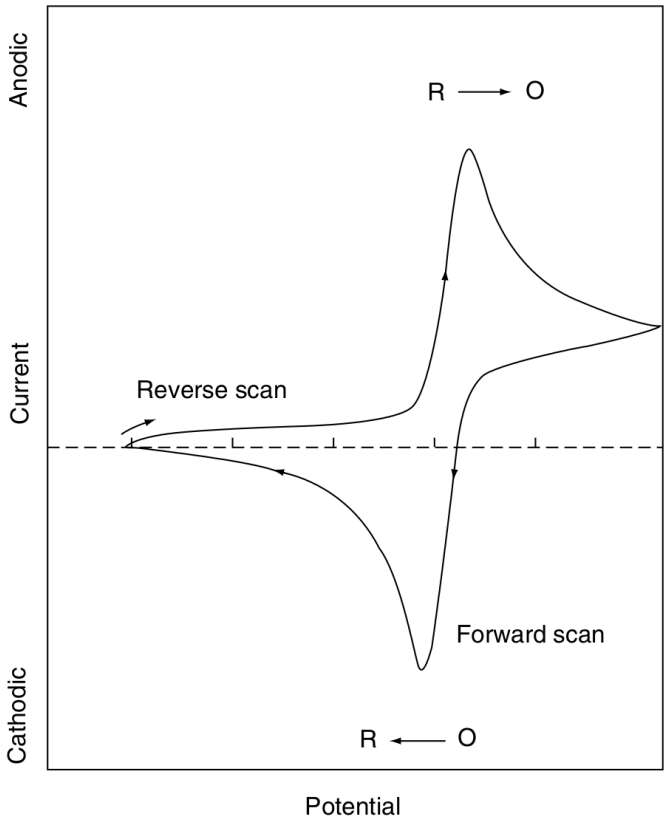

Figure 2.4. Typical cyclic voltammogram for a reversible $O + ne^- \leftrightarrows R$ redox process, during a single potential cycle. "R" represents the reduced form and "O" represent the oxidized form. A negative-going potential scan is chosen for the first half-cycle, starting from a value where no reduction occurs. In CV, the anodic peaks (resulting from oxidation reactions) are positive and the cathodic peaks (resulting from reduction reactions) are negative [16]. This figure was adapted from [16].

2.6.2. Electrochemical studies

CV was used to determine the redox potential of GSU1740 at different pH values (6.0; 7.0 and 8.0). The assays were carried out inside a Faraday cage using a single-chamber, three-electrode system connected to a CHI 440b potentiostat. The cell was equipped with a stirring system and argon inlet entrances, for experiments to be allowed to run in low oxygen environments.

The three-electrode system encompasses: (i) the working electrode, capable of selectively measuring the activity of a particular ionic species, on which the electrochemical reaction occurs, (ii) the reference electrode, which provides a highly stable potential throughout the electrochemical reaction and (iii) the auxiliary electrode, which is used to ensure a flowing current to close the circuit. In protein electrochemistry, it is very common to use pyrolytic graphite (PG) working electrodes, since they have been proved to be especially useful for probing redox-active proteins, including those in the *c*-type cytochrome family [18]. The potential of the reference electrodes is known and unaffected by changes in the investigated sample conditions, and one of the most commonly used is the silver chloride (Ag/AgCl, 3M KCl) electrode. The auxiliary electrodes are usually made of well-conductive and inert materials, such as platinum [16]. In the present work, a saturated silver/silver chloride (Ag/AgCl), with a potential of +197 mV with respect to Normal Hydrogen Electrode (NHE) at room temperature was used as a reference electrode. The counter electrode was a platinum wire and the working electrode was a pyrolytic graphite disk with 3mm diameter and was first polished with two different grades of alumina (1 and 0.3 μm), subjected to a Millipore water ultra-sound bath for 2 minutes, and washed thoroughly with Millipore water. After the working electrode was dried, 5 μL of cytochrome GSU1740 solution were placed on top of the electrode. The solution added was let to evaporate (solvent casting technique), at room temperature, until it reached approximately half of the initial volume. Next, the protein was entrapped using a 3.5 kDa MWCO cellulose membrane (spectra/Pro) and fitted with two O-rings, in order for the protein solution to form a uniform thin layer on the electrode surface. The electrodes were then immersed into the supporting electrolyte. After that, the electrolyte was degassed with a continuous flow of argon for least 30 minutes. All the assays were performed in an anaerobic environment, with a positive argon pressure on the electrochemical cell headspace, as previously described [19].

2.7. References

[1] Y.Y. Londer, P.R. Pokkuluri, D.M. Tiede, M. Schiffer, Production and preliminary characterization of a recombinant triheme cytochrome c_7 from *Geobacter sulfurreducens* in *Escherichia coli*, Biochim. Biophys. Acta, 1554 (2002) 202–211.

[2] T. Unger, Y. Jacobovitch, A. Dantes, R. Bernheim, Y. Peleg, Applications of the Restriction Free (RF) cloning procedure for molecular manipulations and protein expression, J. Struct. Biol., 172 (2010) 34–44.

[3] F. van den Ent, J. Löwe, RF cloning: A restriction-free method for inserting target genes into plasmids, J. Biochem. Biophys. Methods, 67 (2006) 67–74.

[4] P.C. Portela, T.M. Fernandes, J.M. Dantas, M.R. Ferreira, C.A. Salgueiro, Biochemical and functional insights on the triheme cytochrome PpcA from *Geobacter metallireducens*, Arch. Biochem. Biophys., 644 (2018) 8–16.

[5] P.R. Pokkuluri, Y.Y. Londer, N.E.C. Duke, J. Erickson, M. Pessanha, C.A. Salgueiro, M. Schiffer, Structure of a novel c_7-type three-heme cytochrome domain from a multidomain cytochrome *c* polymer, Protein Sci., 13 (2004) 1684–1692.

[6] J.M. Dantas, D.M. Tomaz, L. Morgado, C.A. Salgueiro, Functional characterization of PccH, a key cytochrome for electron transfer from electrodes to the bacterium *Geobacter sulfurreducens*, FEBS Lett., 587 (2013) 2662–2668.

[7] K. Ohno, M. Tanaka, H. Ino, H. Suzuki, M. Tashiro, T. Ibi, K. Sahashi, A. Takahashi, T. Ozawa, Direct DNA sequencing from colony: analysis of multiple deletions of mitochondrial genome, Biochim. Biophys. Acta BBA - Gene Struct. Expr., 1090 (1991) 9–16.

[8] L. Thöny-Meyer, Biogenesis of Respiratory Cytochromes in Bacteria, Microbiol. Mol. Biol. Rev., 61 (1997) 337–376.

[9] L. Thöny-Meyer, F. Fischer, P. Künzler, D. Ritz, H. Hennecke, *Escherichia coli* Genes Required for Cytochrome *c* Maturation, J. Bacteriol., 177 (1995) 4321–4326.

[10] M.J. Edelmann, Strong Cation Exchange Chromatography in Analysis of Posttranslational Modifications: Innovations and Perspectives, J. Biomed. Biotechnol., 2011 (2011) 1–7.

[11] I.C. Guerrera, O. Kleiner, Application of Mass Spectrometry in Proteomics, Biosci. Rep., 25 (2005) 71–93.

[12] G.R. Moore, G.W. Pettigrew, Cytochromes *c*: Evolutionary, Structural and Physicochemical Aspects, Springer-Verlag Berlin Heidelberg, 1990.

[13] G.S. Rule, T.K. Hitchens, Fundamentals of protein NMR spectroscopy, Springer, Dordrecht, 2006.

[14] N.J. Greenfield, Using circular dichroism spectra to estimate protein secondary structure, Nat. Protoc., 1 (2006) 2876–2890.

[15] A. Kaifer, M. Gómez-Kaifer, Supramolecular Electrochemistry, Wiley-VCH, Weinheim, 1999.

[16] J. Wang, Analytical electrochemistry, 3. ed, Wiley-VCH, Hoboken, NJ, 2006.

[17] P.T. Kissinger, W.R. Heineman, Laboratory Techniques in Electroanalytical Chemistry, 2. ed, Marcel Dekker, New York, 1996.

[18] H. Allen, O. Hill, Bio-electrochemistry, Pure & Appl. Chem., 59 (1987) 743–748.

[19] L.R. Teixeira, J.M. Dantas, C.A. Salgueiro, C.M. Cordas, Thermodynamic and kinetic properties of the outer membrane cytochrome OmcF, a key protein for extracellular electron transfer in *Geobacter sulfurreducens*, BBA - Bioenergetics, 1859 (2018) 1132–1137.

3. RESULTS AND DISCUSSION

3.1. Optimization of the protein expression

3.1.1. *E. coli* strain selection

Six strains of *E. coli* cells containing plasmid pEC86 (BL21 (DE3), SF110, JM109, JCB7123, C43 (DE3), and Tuner (DE3)) were transformed with the expression vector containing the GSU1740 gene sequence for mature proteins (PCR product results in Appendix 3), but only four of them yielded colonies in the solid medium: BL21 (DE3), JM109, JCB7123, and Tuner (DE3). The colonies obtained from these four strains were then transferred to liquid medium, but only three were successful: BL21 (DE3), JM109 and Tuner (DE3).

3.1.2. Production of recombinant proteins

In order to gather some insights on which possible optimization could be made in the expression protocol different variables were tested (see on next page).

The resulting cell cultures obtained with the three strains previously mentioned, were then induced with IPTG (100 μM) for protein overexpression and the presence of the desired cytochrome was confirmed by SDS-PAGE stained with TMBZ/H_2O_2 to detect hemes (Fig. 3.1). It was not clear in this first gel, but it seemed that in all three strains, 2 hours after the induction the cells were already expressing a protein with approximately 15 kDa but not the GSU1740 protein (≃10 kDa). The latter apparently only expressed after overnight incubation.

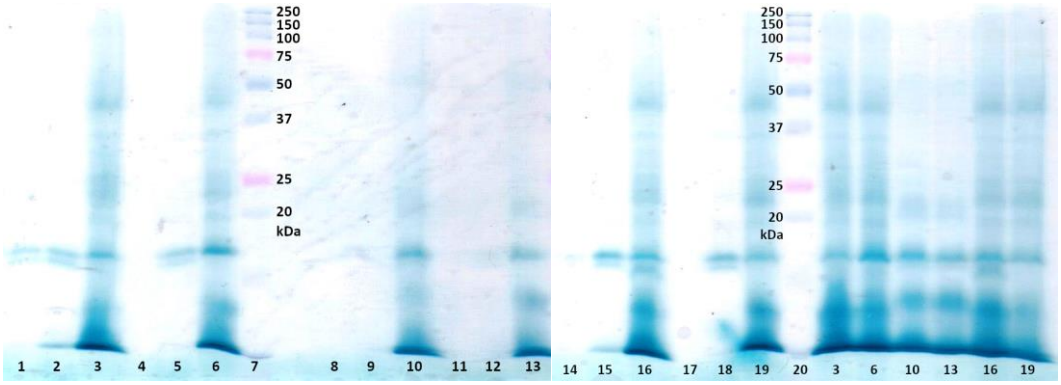

Figure 3.1. First cell culture cytochrome GSU1740 expression survey by SDS-PAGE gel 15 %, stained with TMBZ/H_2O_2 to detect hemes. Samples taken of BL21(DE3)/pEC86/pVA203 before induction with IPTG at OD_{600nm} 0.7 (lane 1) and 1.5 (lane 4), 2h after induction at OD_{600nm} 0.7 (lane 2) and 1.5 (lane 5) and 18-20h after induction at OD_{600nm} 0.7 (lane 3) and 1.5 (lane 6). Samples taken of JM109/pEC86/pVA203 before induction with IPTG at OD_{600nm} 0.7 (lane 8) and 1.5 (lane 11), 2h after induction at OD_{600nm} 0.7 (lane 9) and 1.5 (lane 12) and 18-20h after induction at OD_{600nm} 0.7 (lane 10) and 1.5 (lane 13). Samples taken of Tuner (DE3)/pEC86/pVA203 before induction with IPTG at OD_{600nm} 0.7 (lane 14) and 1.5 (lane 17), 2h after induction at OD_{600nm} 0.7 (lane 15) and 1.5 (lane 18) and 18-20h after induction at OD_{600nm} 0.7 (lane 16) and 1.5 (lane 19). Lanes 7 and 20 correspond to the protein marker *Precision Plus Protein™ Dual Xtra Prestained Protein Standards* (Bio-Rad) (see Appendix 2A for details).

The results obtained (Fig. 3.1) indicate that the most efficient strain for the expression of cytochrome GSU1740 was *E. coli* BL21 (DE3), containing the pEC86 plasmid that codes for all the machinery required for the hemes incorporation [1,2].

The next test was the volume/aeration of the 2xYT medium used for aerobic growth. The first two rounds of cell cultures were grown in 800 mL of 2xYT medium in 2-liter erlenmeyers and a third round (Fig. 3.2) was grown in 500 mL of 2xYT medium in 2-liter erlenmeyers, to facilitate the air flow. The cell cultures that were grown in 500 mL of 2xYT medium did not show clearly a more intense pink colour, suggesting that the improved air flow does not significantly affect the protein expression levels.

Another optimized parameter included the amount of IPTG used for protein expression induction (50, 100 and 200 µM). In a second round of expression and purification of GSU1740. In this case, the protein expression was performed in the same conditions, with the only difference being the IPTG concentration. The higher IPTG concentration (200 µM) did not affect the intensity of the band in the SDS-PAGE gel (Fig. 3.2) or the periplasmic fraction colour (not shown). The lower (50 µM) had a negative impact on both.

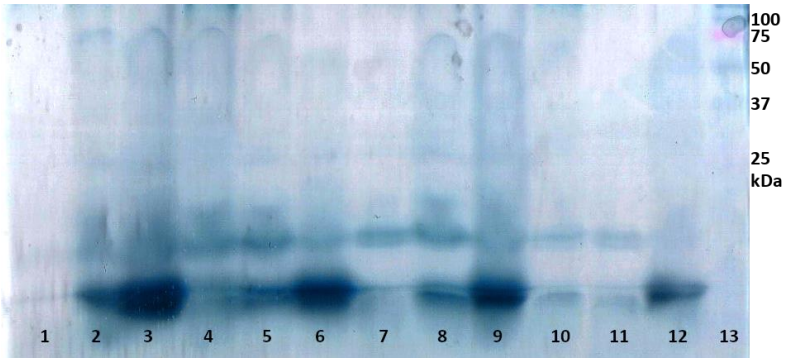

Figure 3.2. Third round of cell cultures cytochrome GSU1740 expression survey by SDS-PAGE gel 15 %, stained with TMBZ/H_2O_2 to detect hemes. Samples taken 2h after induction at OD_{600nm} 0.7, stable 30 ºC, with IPTG 100 µM (lane 1), 50 µM (lane 4), and 200 µM (lane 7), and with IPTG 100 µM at unstable 20-30 ºC (lane 10). 4h after induction at OD_{600nm} 0.7, stable 30 ºC, with IPTG 100 µM (lane 2), 50 µM (lane 5), and 200 µM (lane 8), and with IPTG 100 µM at unstable 20-30 ºC (lane 11). Samples taken 20-22h after induction at OD_{600nm} 0.7, stable 30 ºC, with IPTG 100 µM (lane 3), 50 µM (lane 6), and 200 µM (lane 9), and with IPTG 100 µM at unstable 20-30 ºC (lane 12); Lane 13: protein marker *Precision Plus Protein™ Dual Xtra Prestained Protein Standards* (Bio-Rad) (see Appendix 2A for details).

3.2. Optimization of the GSU1740 protein purification

The cytochrome GSU1740 purification was planned to consist of a cation exchange chromatography followed by a size exclusion chromatography, based on previous works on the monoheme cytochrome PccH of *G. sulfurreducens* [3].

For that purpose, some optimization had to be done first, in order to determine the best purification protocol. In both chromatography steps, the purity of eluted fractions was analysed by SDS-PAGE (15% acrylamide/bis-acrylamide).

The buffers tested all had a pH below the predicted isoelectric point (pI) of 8.9 for the cytochrome GSU1740, with the objective of generating a net positive charge on the protein. This is required for the binding of it to the negatively charged cationic exchange resin. Afterwards, elution was achieved by

gradually increasing ionic strength of the buffer using NaCl. The proteins were eluted in order of their increasing net charges.

A considerable amount of protein did not bind to the column in the first cation exchange chromatography and the peaks of the eluted protein that did bind were not well resolved (Fig. 3.3).

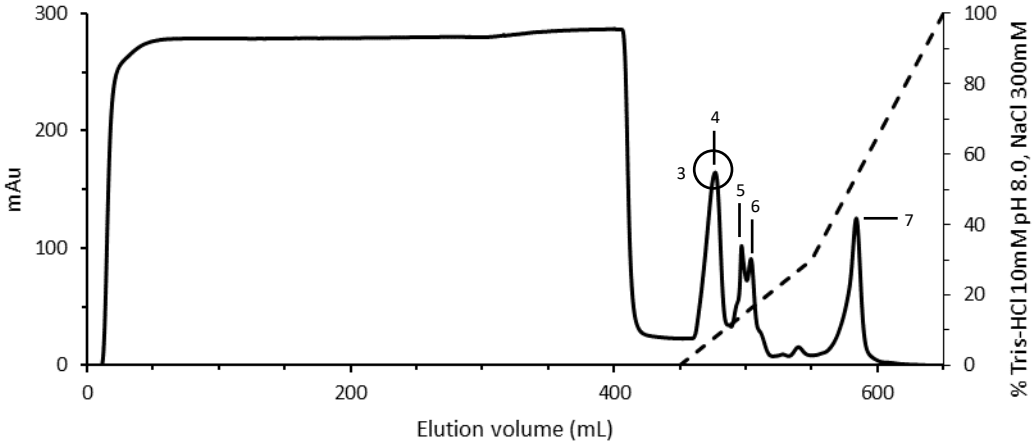

Figure 3.3. Cation exchange chromatogram, obtained using two 5 mL *Bio-Scale Mini UNOsphere S* cartridges (Bio-Rad) connected and equilibrated with 10 mM Tris-HCl pH 8.0 and eluted with a 10 column volumes NaCl gradient (0-300 mM) at a flow rate of 1.0 mL/min. The primary and secondary y-axis report the variation of absorbance at 280 nm (solid line) and the NaCl gradient profile (dashed line), respectively. Labels 4, 5, 6 and 7: samples taken from the centre of each peak and evaluated by SDS-PAGE (Fig. 3.4). Mark 3 (circle): the peak evaluated by SDS-PAGE (Fig. 3.9).

The analysis of the purity of the sample is indicated in Figure 3.4.

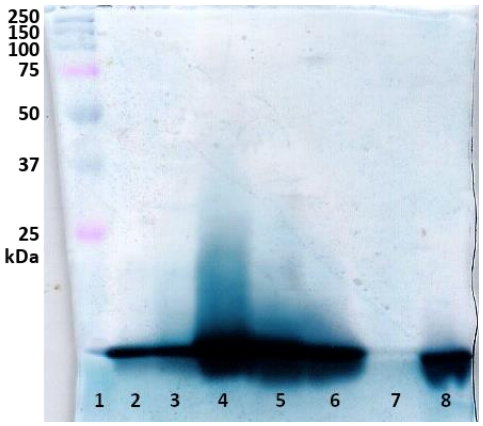

Figure 3.4. Cytochrome GSU1740 purity evaluation by SDS-PAGE gel 15 %, stained with TMBZ/H_2O_2 to detect hemes. Lane 1: protein marker *Precision Plus Protein™ Dual Xtra Prestained Protein Standards* (Bio-Rad) (see Appendix 2A for details). Lane 2: column load sample. Lane 3: column flow through sample. Lanes 4-7: fractions of the centre of each peak labelled in Figure 3.3. 8: sample of the periplasmic fraction isolated from a second cell culture of identical cells grown in 500 mL of 2xYT medium.

Not all the protein binded to the *Bio-Scale Mini UNOsphere S* (Bio-Rad) column, since the presence of it is perfectly visible in the flow through sample (Fig. 3.4). Possible causes for this: column saturation and weak binding to the column. Following these results, further optimizations of the purification process were pursuit.

With the objective of increasing the protein bind to the column and to improve the purification yields, the buffer 10 mM Tris-HCl at pH 7.5 and the cation exchange column *Econo-Pac Hitrap SP HP* (GE) were tested (Figs. 3.5, 3.6, 3.7, 3.8) and all the fractions collected were analysed by SDS-PAGE (15%) (Fig. 3.9). *Econo-Pac Hitrap SP HP* (GE) column differs from the *Bio-Scale Mini UNOsphere S* (Bio-Rad) column manly in the resin it is packed with. The smaller pH values tested yield a higher net positive charge on the surface of the protein and, therefore, it is expected to contribute to a stronger protein's binding to the column.

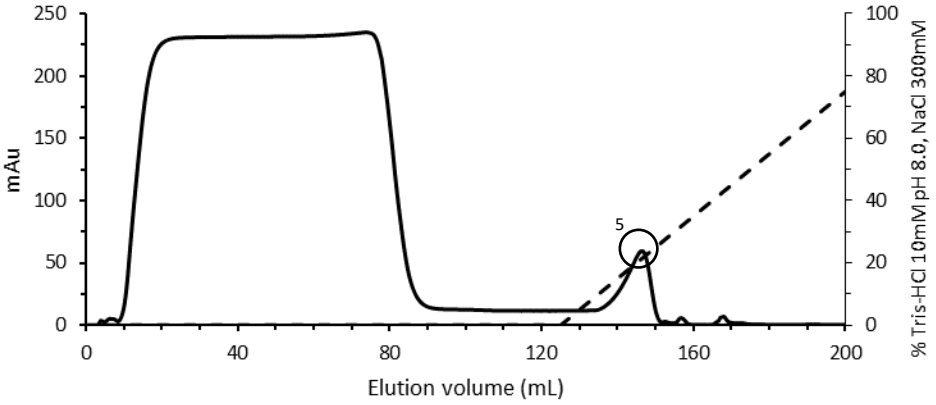

Figure 3.5. Cation exchange chromatogram for column flow through collected in the first chromatography (Fig. 3.3), obtained using two 5 mL *Econo-Pac Hitrap SP HP* cartridges (GE) connected and equilibrated with 10 mM Tris-HCl pH 8.0 and eluted with a 10 column volumes NaCl gradient (0-300 mM) at a flow rate of 0.7 mL/min. The primary and secondary y-axis report the variation of absorbance at 280 nm (solid line) and the NaCl gradient profile (dashed line), respectively. Mark 5: peak evaluated by SDS-PAGE (lane 5 in Fig. 3.9).

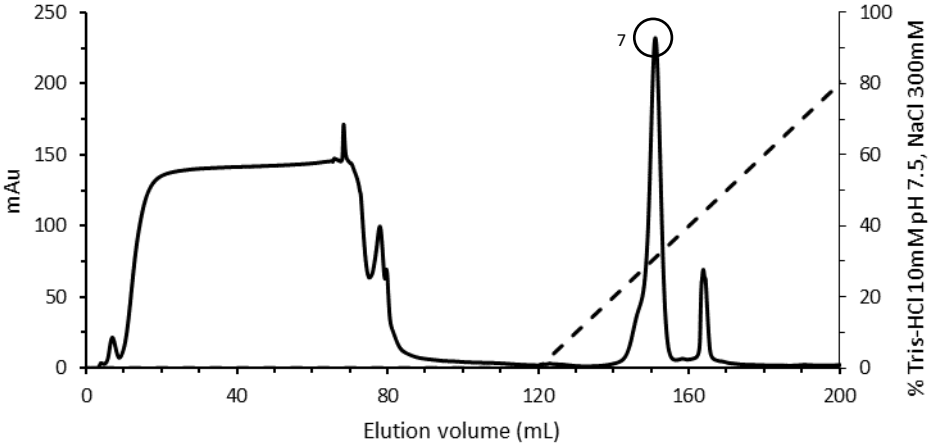

Figure 3.6. Cation exchange chromatogram for column flow through collected in the first chromatography (Fig. 3.3), obtained using two 5 mL *Econo-Pac Hitrap SP HP* cartridges (GE) connected and equilibrated with 10 mM Tris-HCl pH 7.5 and eluted with a 10 column volumes NaCl gradient (0-300 mM) at a flow rate of 0.7 mL/min. The primary and secondary y-axis report the variation of absorbance at 280 nm (solid line) and the NaCl gradient profile (dashed line), respectively. Mark 7: peak evaluated by SDS-PAGE (lane 7 in Fig. 3.9).

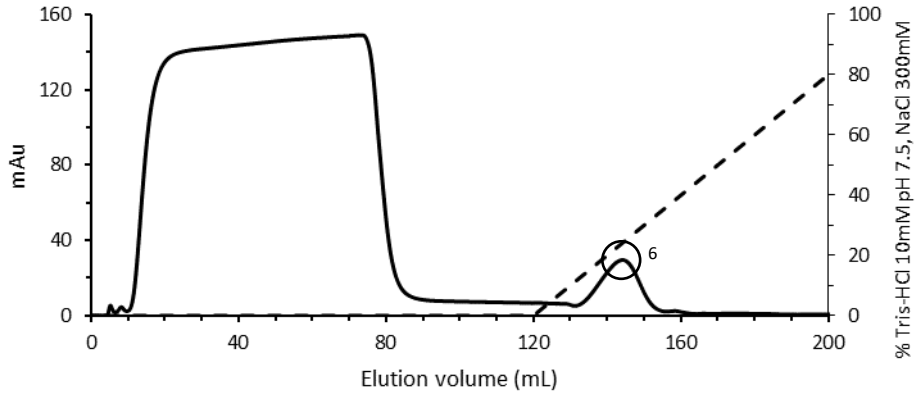

Figure 3.7. Cation exchange chromatogram for column flow through collected in the first chromatography (Fig. 3.3), obtained using two 5 mL *Bio-Scale Mini UNOsphere S* cartridges (Bio-Rad) connected and equilibrated with 10 mM Tris-HCl pH 7.5 and eluted with a 10 column volumes NaCl gradient (0-300 mM) at a flow rate of 0.7 mL/min. The primary and secondary y-axis report the variation of absorbance at 280 nm (solid line) and the NaCl gradient profile (dashed line), respectively. Mark 6: peak evaluated by SDS-PAGE (lane 6 in Fig. 3.9).

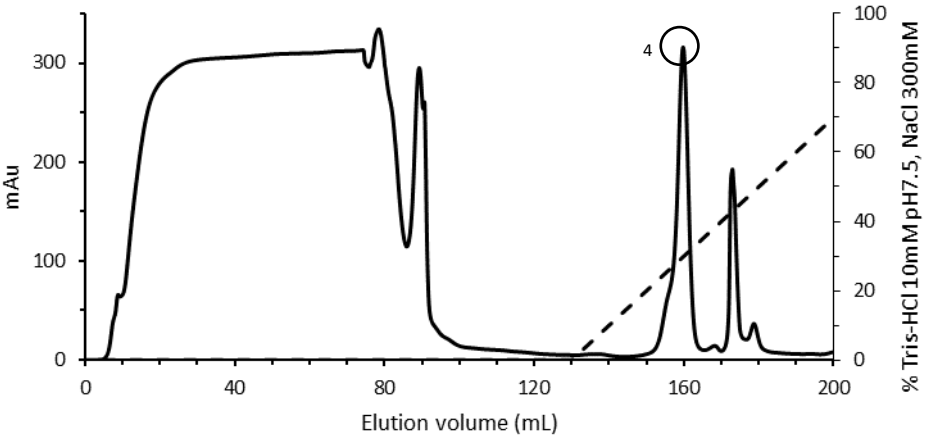

Figure 3.8. Cation exchange chromatogram for the periplasmic fraction of the second cell culture grown in 500 mL of 2xYT medium in a 2-liter flask, obtained using two 5 mL *Econo-Pac Hitrap SP HP* cartridges (GE) connected and equilibrated with 10 mM Tris-HCl pH 7.5 and eluted with a 10 column volumes NaCl gradient (0-300 mM) at a flow rate of 0.7 mL/min. The primary and secondary y-axis report the variation of absorbance at 280 nm (solid line) and the NaCl gradient profile (dashed line), respectively. Mark 4:peak evaluated by SDS-PAGE (lane 4 in Fig. 3.9).

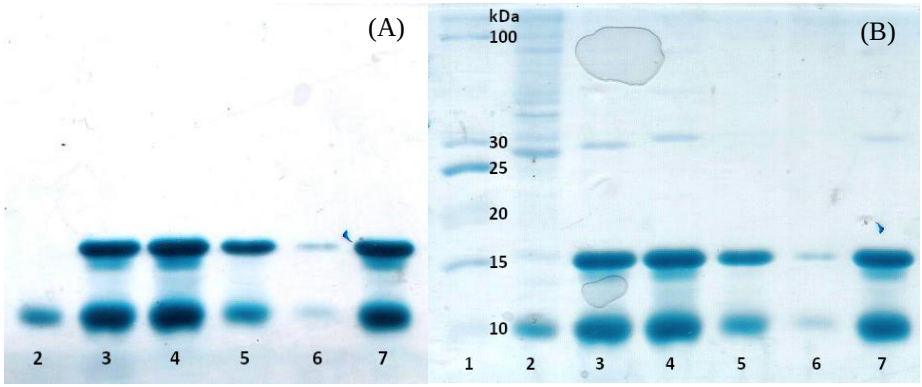

Figure 3.9. Cytochrome GSU1740 purity evaluation by SDS-PAGE gel 15 %, stained with TMBZ/H_2O_2 to detect hemes (A) and with BlueSafe (B). Lane 1: protein marker *Precision Plus Protein™ Dual Xtra Prestained Protein Standards* (Bio-Rad) (see Appendix 2A for details). Lane 2: column load fraction. Lanes 3-7: samples of the peaks marked in Figures 3.3, 3.5, 3.6, 3.7 and 3.8.

By analysing all the previous chromatograms (Figs. 3.3 to 3.8), it's possible to conclude that most of the protein that binds to the column elute approximately at 30 % of the ionic force gradient (NaCl 0-300 mM). It's also possible to observe that the best chromatogram peak resolution was obtained using the *Econo-Pac Hitrap SP HP* cartridges (GE) equilibrated with 10 mM Tris-HCl at pH 7.5 (Figures 3.6 and 3.8). Only the peaks with brown-red coloured fractions were analysed by SDS-PAGE (15%) (Fig. 3.9) and the results confirmed this was the best cation exchange chromatography protocol obtained so far.

These results also confirmed that proteins with molecular weight of 10 and 15 kDa were obtained probably due to their similar pI.

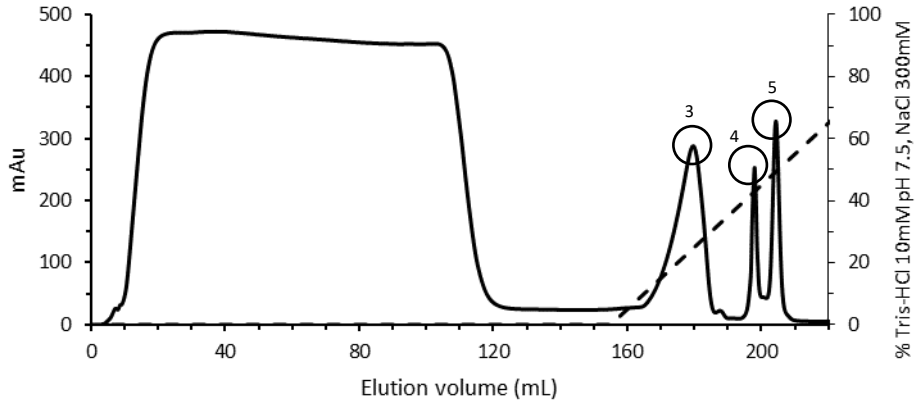

Figure 3.10. Cation exchange chromatogram for a portion of the periplasmic fraction of the third cell culture, obtained using two 5 mL *Econo-Pac Hitrap SP HP* cartridges (GE) connected and equilibrated with 10 mM Tris-HCl pH 7.5 and eluted with a 10 column volumes NaCl gradient (0-300 mM) at a flow rate of 0.7 mL/min. The primary and secondary y-axis report the variation of absorbance at 280 nm (solid line) and the NaCl gradient profile (dashed line), respectively. Marks 3-5: peaks evaluated by SDS-PAGE (lanes 3-5 in Fig. 3.12).

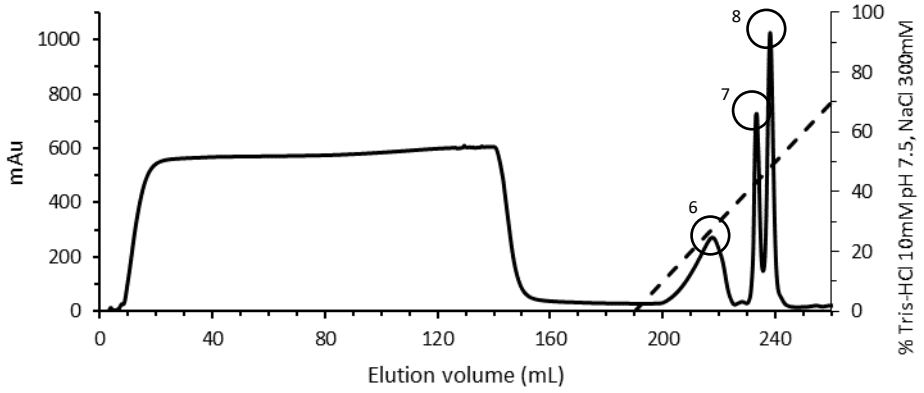

Figure 3.11. Cation exchange chromatogram for another portion of the periplasmic fraction of the third cell culture mixed with the flow through of the previous chromatography (Figure 3.10), obtained using two 5 mL *Econo-Pac Hitrap SP HP* cartridges (GE) connected and equilibrated with 10 mM Tris-HCl pH 7.5 and eluted with a 10 column volumes NaCl gradient (0-300 mM) at a flow rate of 0.7 mL/min. The primary and secondary y-axis report the variation of absorbance at 280 nm (solid line) and the NaCl gradient profile (dashed line), respectively. Marks 6-8: peaks evaluated by SDS-PAGE (lanes 6-8 in Figure 3.12).

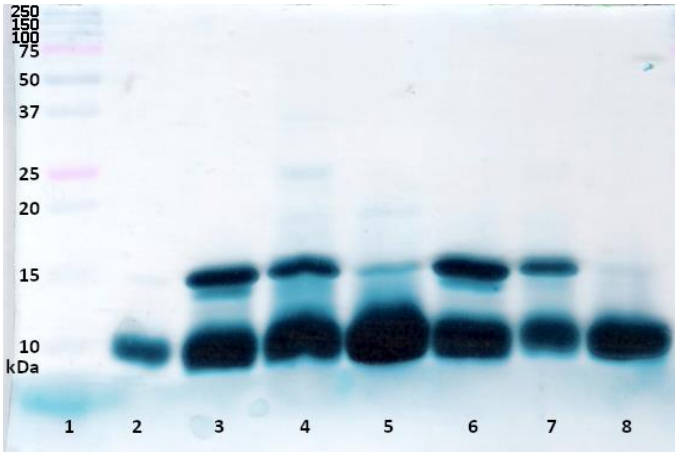

Figure 3.12. Cytochrome GSU1740 purity evaluation by SDS-PAGE gel 15 %, stained with TMBZ/H_2O_2 to detect hemes. Lane 1: protein marker *Precision Plus Protein™ Dual Xtra Prestained Protein Standards* (Bio-Rad) (see Appendix 2A for details). Lane 2: column flow through of the last chromatography (Figure 3.11). Lanes 3-8: samples of the peaks marked in Figures 3.10 and 3.11.

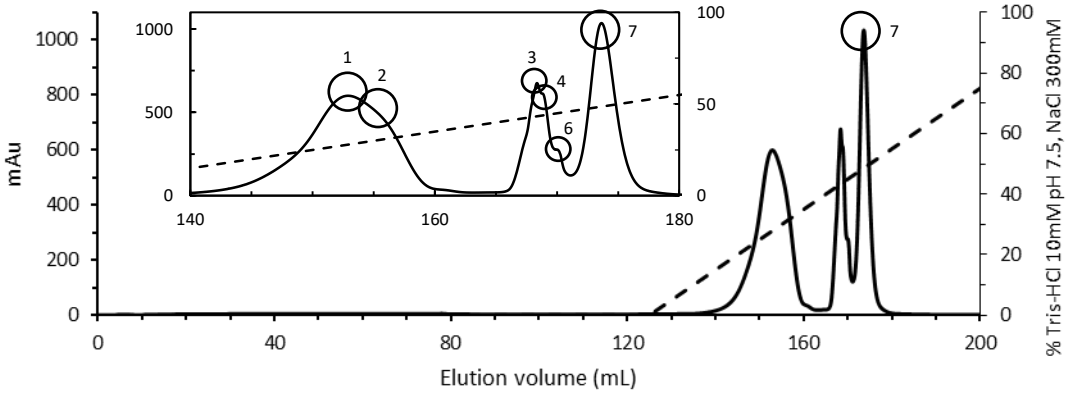

Figure 3.13. Cation exchange chromatogram for the mixture of the protein fractions collected in last two chromatographic essays (Figure 3.10, 3.11), obtained using two 5 mL *Econo-Pac Hitrap SP HP* cartridges (GE) connected and equilibrated with 10 mM Tris-HCl pH 7.5 and eluted with a 10 column volumes NaCl gradient (0-300 mM) at a flow rate of 0.7 mL/min. The primary and secondary y-axis report the variation of absorbance at 280 nm (solid line) and the NaCl gradient profile (dashed line), respectively. The inset shows a region of the same spectra in greater detail. Marks 1-7: peaks evaluated by SDS-PAGE (lanes 1-7 in Figure 3.14), five of them not well resolved and one well resolved (peak marked as 7).

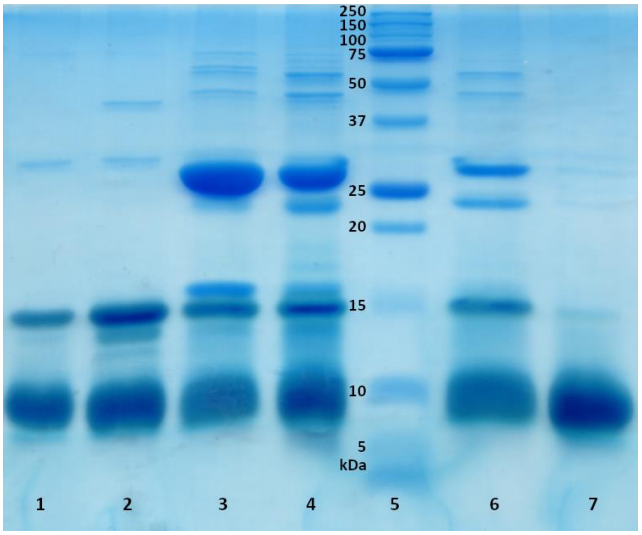

Figure 3.14. Cytochrome GSU1740 purity evaluation by SDS-PAGE gel 15 %, stained with BlueSafe. Lanes 1-4, 6, 7: samples of the peaks marked in Figure 3.13. Lane 5: protein marker *Precision Plus Protein™ Dual Xtra Prestained Protein Standards* (see Appendix 2A for details).

The fractions obtained were further analysed by SDS-PAGE (15%) and the results demonstrated that GSU1740 (assuming that was the only brown protein with 10 kDa to bind to the chromatographic column) was found in all the fractions resulting from the cation exchange chromatography performed on the periplasmic fraction of the *E. coli* BL21(DE3) cells (Figure 3.14).

In the size exclusion chromatography step, the first test was performed using the fractions 3, 4, 5 and 7 (Figure 3.9) pooled together. This sample was concentrated to approximately 1 mL before being injected into the column and eluded at a flow rate of 0.7 mL/min. The resulting peak contained the same two periplasmic proteins with approximately with 10 and 15 kDa, respectively (Figure 3.15).

Another test was done using the fractions of peak 1 and 2 (Figure 3.13) pooled together, injected into the size exclusion chromatography column and eluded at a flow rate of 0.3 mL/min. Samples taken from different eluted fractions of the not well resolved peak registered in the chromatogram (Appendix 3)

(similar to the chromatogram in Figure 3.15) were analysed by SDS-PAGE (15%) (data not shown) and the same two 10 and 15 kDa proteins were observed in all of them.

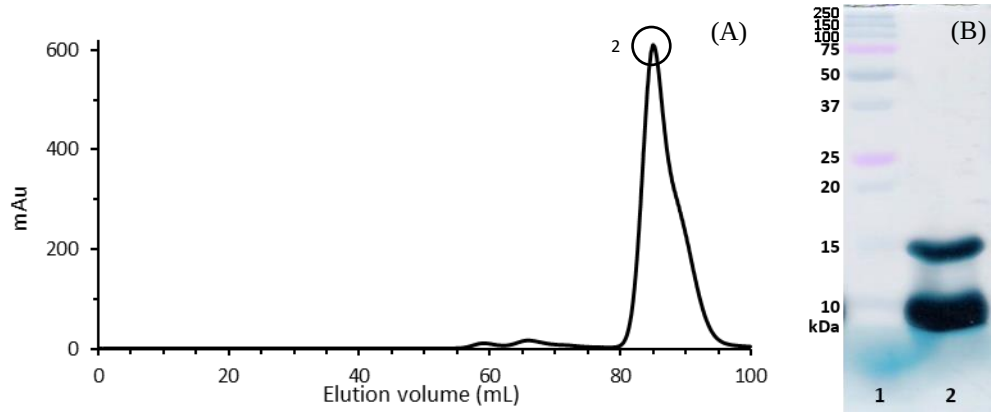

Figure 3.15. (A): Size exclusion chromatogram obtained using a XK 16/70 column (GE Healthcare) packed with *Superdex^{TM} 75* and equilibrated with 100 mM sodium phosphate pH 7.5. Protein was eluted at a flow rate of 0.7 mL/min. (B): Cytochrome GSU1740 purity evaluation by SDS-PAGE gel 15%, stained with TMBZ/H_2O_2 to detect hemes. Lane 1: protein marker *Precision Plus Protein™ Dual Xtra Prestained Protein Standards* (Bio-Rad) (see Appendix 2A for details). Lane 2: sample of the brown-red coloured fractions of the peak pooled together.

The sample 7 in Figure 3.14 was the only one where the presence of GSU1740 was undoubtedly predominant. For this reason, a size exclusion chromatography with the fractions of the well resolved peak 7 (Figure 3.13) pooled together was carried out at flow rate of 1.0 mL/min yielding a single peak (data not shown). The purity was evaluated by SDS-PAGE (15%) (Figure 3.16).

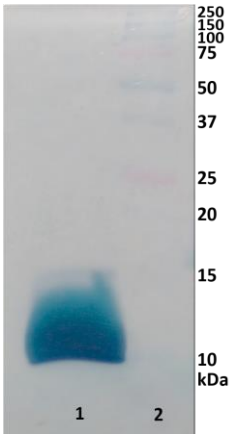

Figure 3.16. Purity evaluation by SDS-PAGE gel 15% with TMBZ/H_2O_2 staining of the cytochrome GSU1740 obtained by size exclusion chromatography using a XK 16/70 column (GE Healthcare) packed with *Superdex^{TM} 75* and equilibrated with 100 mM sodium phosphate pH 7.5. Lane 1: sample of the brown-red coloured fractions pooled together. Lane 2: protein marker *Precision Plus Protein™ Dual Xtra Prestained Protein Standards* (see Appendix 2A for details).

Considering all the results obtained and analysed, for all the different expression and purification tests, the most adequate protocol for GSU1740 expression and purification was established. For protein expression, *E. coli* BL21(DE3) strain should be grown in 2-liter erlenmeyers with 1000 mL of 2xYT medium and induced with 100 μM IPTG at OD_{600nm} of 0.7, followed by overnight incubation at 30 ºC. The best purification results were obtained with a by cation exchange chromatography, using two 5 mL *Econo-Pac Hitrap SP HP* cartridges (GE) connected and equilibrated with 10 mM Tris-HCl pH 7.5, followed by size exclusion chromatography step.

3.3. Molecular mass determination

As described above, the purity of cytochrome GSU1740 was assessed by SDS-PAGE (Fig. 3.16) and confirmed by MALDI-TOF Mass Spectrometry (Laboratory for Biological Mass Spectrometry, Isabel Moura (LBMS-IM)). The theoretical molecular weight (Mw) of cytochrome GSU1740 was calculated according to the amino acid composition of the mature protein, using the pI/Mw tool program on the ExPASy server (https://web.expasy.org/compute_pi), plus 616 Da of one heme group [1]. The mass spectra obtained is indicated in Fig. 3.17. The peak of the pure cytochrome corresponds to a molecular mass of 9361 (± 1Da), which in agreement with the predicted molecular weight for mature cytochrome GSU1740 (9364 Da).

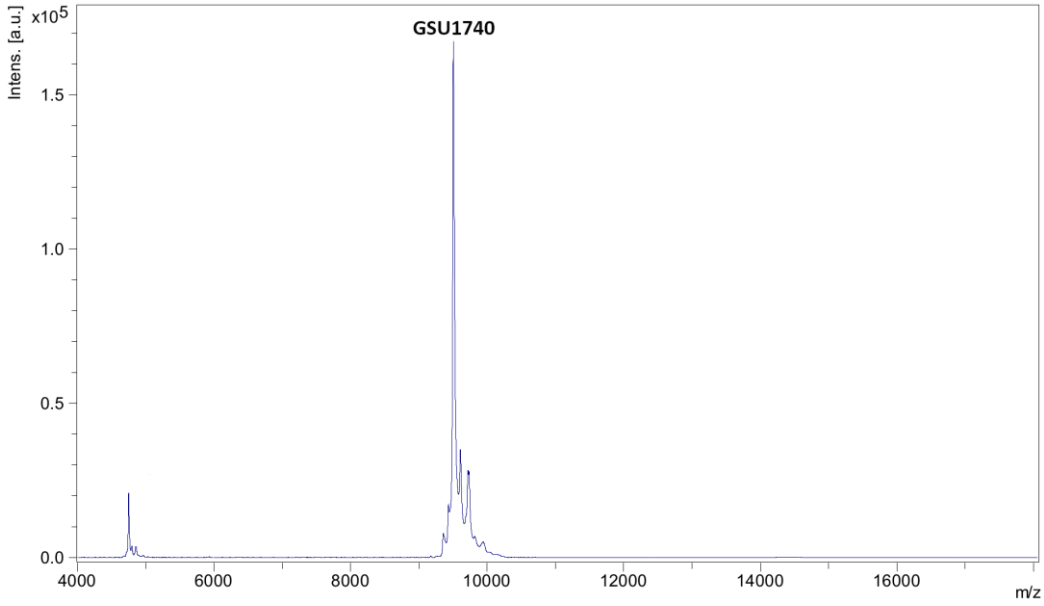

Figure 3.17. MALDI-TOF Mass Spectrometry spectrum for cytochrome GSU1740, 4000 – 18000 m/z (LBMS-IM).

3.4. Protein quantification

The molar extinction coefficient (ε) of purified cytochrome GSU1740 in the reduced form determined, estimated by the Lowry method, was of 9.2 $mM^{-1} \cdot cm^{-1}$.

Knowing this, it was possible to calculate the expression yield of cytochrome GSU1740 under the growth and purification conditions optimized previously. For each litre of culture of *E. coli* BL21(DE3) transformed with the pVA203-GSU1740 plasmid, it was possible to produce and purify 4.3 mg of cytochrome GSU1740.

3.5. Spectroscopic characterization of GSU1740

UV-visible absorption and NMR spectroscopic techniques were used to probe the protein's heme spin-state and the nature of the heme axial ligands of the cytochrome GSU1740.

The optical absorption spectrum of the oxidized and reduced is indicated in Figure 3.17. In the oxidized state (ferricytochrome; Fe^{3+}) the protein has maxima at 403, 499 and 625 nm. In the reduced state ferrocytochrome; Fe^{2+}), the Soret, β and α bands at 419, 525 and 553 nm, respectively.

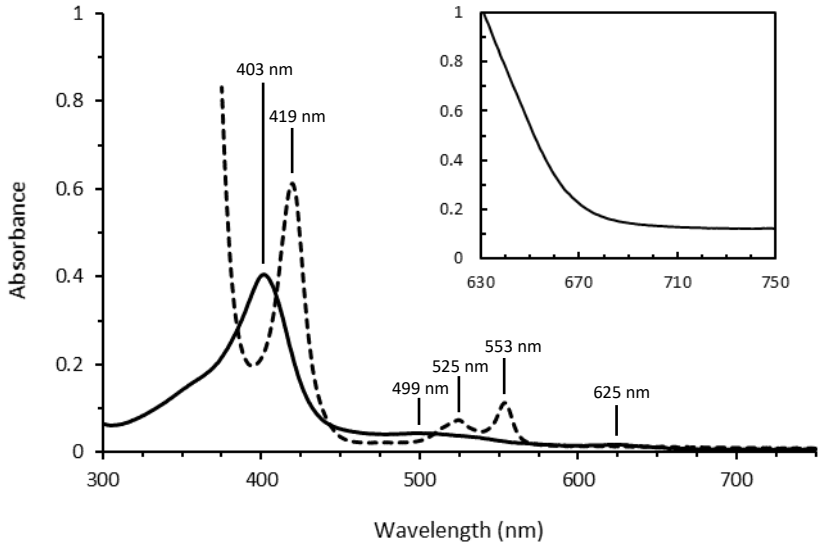

Figure 3.18. UV-visible absorption spectra for cytochrome GSU1740 in the fully oxidized (solid line) and fully reduced (dashed line) states. The maxima of the UV-visible absorption spectra of the cytochrome in the oxidized and reduced states are labelled. The inset shows the near 650nm region of the visible spectra of concentrated GSU1740 in the fully oxidized state.

Compared with the literature, the values of the charge-transfer (CT) bands observed in the UV-visible absorption spectra suggests that the heme group is high-spin in the oxidized state (S = 5/2), with an CT band at 625 nm, and low-spin hexacoordinated in the reduced state (Fe(II), S = 0) [4].

The spin-state of most cytochromes *c* does not change with a variation in the oxidation state. Notable exceptions are the periplasmic heme-containing sensor proteins GSU0582 and GSU0935 from *G. sulfurreducens* [5]. These cytochromes *c* possess one heme with histidine-methionine (His-Met) coordination in the reduced state. The change in the redox state of these sensor proteins is

coupled to a heme spin-state/coordination alteration, as a consequence of the detachment of the Met residue at the heme distal position in the reduced form [5,6]. Therefore, these cytochromes are high-spin and low-spin in the oxidized and reduced states, respectively. The UV-visible absorption spectra of these cytochromes in the oxidized state both present a CT band with maximum at 623 nm [5]. In the UV-visible absorption spectra of oxidized low spin cytochromes, a CT band at 695 nm is characteristic of His-Met iron axial coordination, which is absent in hemes with His-His axial coordination [4]. Theorell and Åkesson [7,8] first observed a weak 695 nm absorbance band in a ferricytochrome *c*. Further studies confirmed that this band is sensitive to pH and to the conformational state of the protein [9,10,11]. The CT band at 695 nm was not observed for cytochrome of this study (inset in Figure 3.17). Most studied cytochromes where it was observed a 695 nm band in the UV-visible absorption spectra contain a methionine axial ligand and the displacement of this ligand is coincident with the loss of the 695 nm band, but the absence of it does not mean that the GSU1740 heme is not coordinated with a methionine residue.

Considering the above mentioned, one hypothesis that explains the observed spectral features of GSU1740 (Figure 3.17) is that the heme is axially coordinated by histidine and methionine residues (His-Met) in the low-spin reduced state, which becomes high-spin in the oxidized state, probably due to the detachment of the axial methionine. In this case the heme become pentacoordinated (no ligand) or hexacoordinated if the methionine residue is replaced by a water molecule (His-H_2O). In fact, there are reports in the literature that match the proposed hypothesis for GSU1740. The cytochrome *c* from *Wolinella succinogenes* has a His-Met heme group a low-spin state in the reduced form and a mixture of high- and low-spin states in the oxidized form [12]. However, the precise heme axial coordination has to be confirmed by EPR and NMR experiments, as previously described [5,12].

NMR is a very powerful technique to identify the spin-state of heme groups in proteins. In the NMR spectra, the signals appear in quite distinct spectral regions, depending upon the spin state of the hemes. In the paramagnetic oxidized state, the 1D ^{1}H-NMR spectra of high-spin cytochromes display extremely broad signals and some frequencies above 40 ppm (usually belonging to heme methyl substituents). Low-spin cytochromes, on the other end, present narrower spectral windows, with the main heme substituents frequencies ranging from 8 to 35 ppm. In the diamagnetic reduced state, 1D ^{1}H-NMR spectra are also quite distinct for high- and low-spin cytochromes. In fact, high-spin hemes present wider spectral regions (ranging from -15 up to 30 ppm) than low-spin ones (ranging from -5 up to 10 ppm).

The signals of oxidized form of GSU1740 in the 1D ^{1}H-NMR spectrum are very broad and cover a wide spectral region, namely from 10 ppm to above 45 ppm (Figure 3.19.(A)). This is in line with the observation made by UV-visible absorption spectroscopy suggesting that the cytochrome is paramagnetic in the oxidized state and contains a high-spin heme.

The 1D ^{1}H-NMR spectrum obtained for reduced form (Figure 3.19.(B)) presents a three-proton intensity peak at approximately -3 ppm and several one proton intensity peaks in the same spectral region which might indicate that a methionine is in fact the axial ligand of the heme group in cytochrome GSU1740.

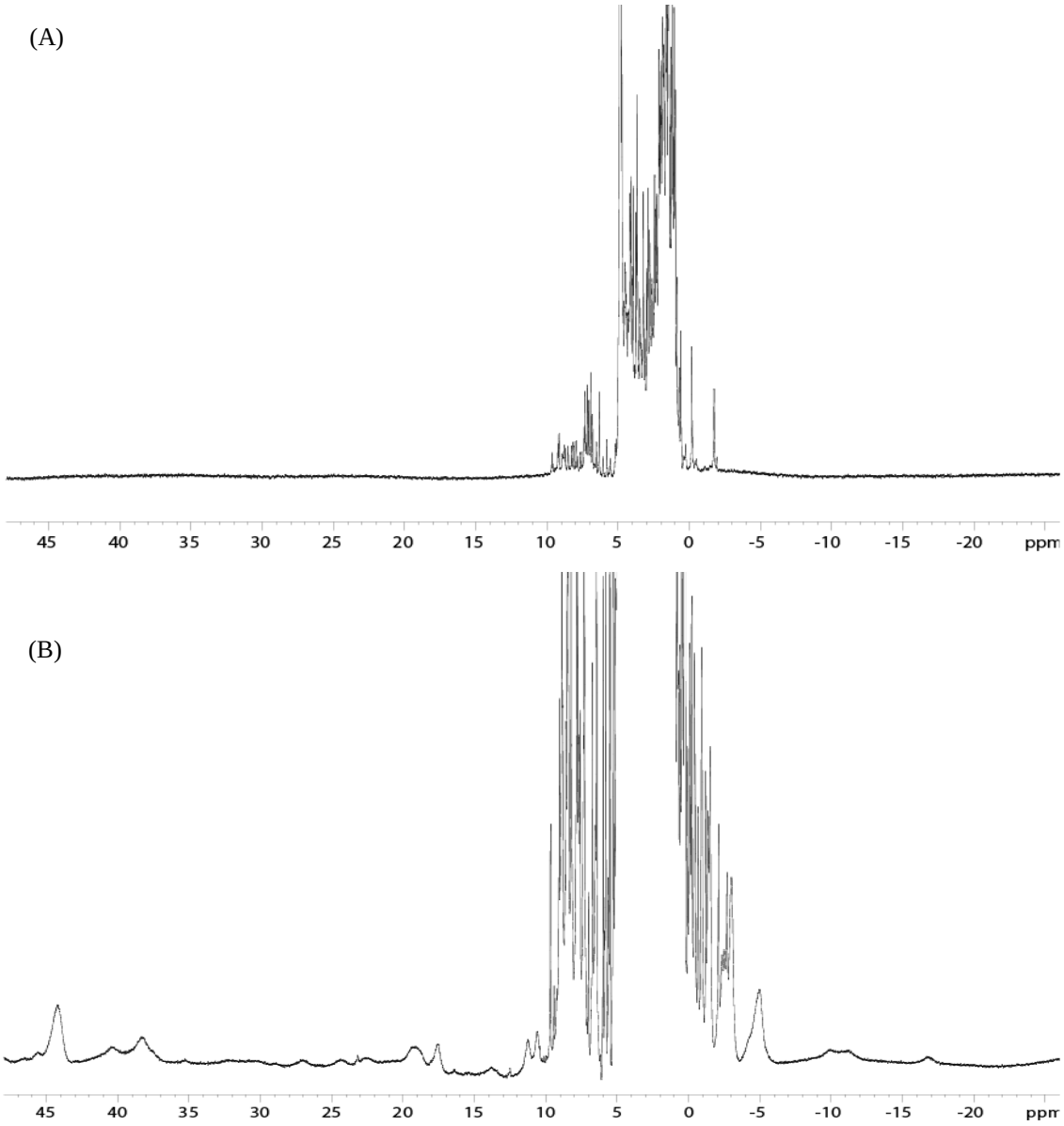

Figure 3.19. NMR spectra for cytochrome GSU1740 in the fully reduced (Fe(II), S = 0) (A) and fully oxidized (Fe(III), S = 5/2) (B) states. Reduction of the sample was achieved with direct addition of sodium dithionite powder to the NMR tube containing GSU1740 (around 20 μM).

Considering all the NMR and UV-visible absorption data obtained the cytochrome GSU1740 heme group appears to have His-Met axial coordination, which needs to be structurally confirmed in the future.

Knowledge of protein structure is fundamental to our understanding of biological function of proteins. There are four levels of protein structure. Each protein has a defined sequence of amino acid residues, which constitutes the first level of organization and is designated as the primary structure. The next level, the secondary structure, refers to regular arrangements of the backbone of the polypeptide chain into α-helix, β sheet, and β turn. The folding of segments of the secondary structure into a compact molecule for the entire polypeptide chain is called the tertiary structure. Those proteins with subunits arranged in a regular manner are said to have the fourth level of organization, the quaternary structure [13].

All-α proteins show a strong double minimum at 222 and 208-210 nm and a stronger maximum at 191-193 nm, which are characteristic of an α-helix (Figure 3.19). The intensities of the three CD bands

reflect the amount of helicity in the proteins. Thus, highly helical myoglobin and hemerythrin show higher intensities than less helical parvalbumin and cytochrome *c* [13].

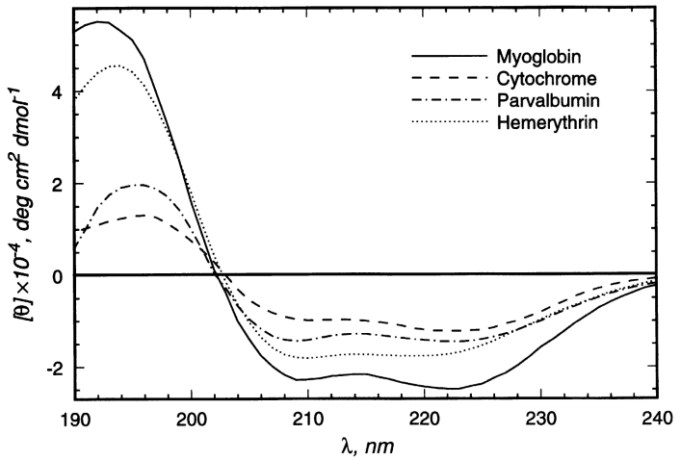

Figure 3.20. Representative CD spectra of all-α proteins (Venyaminov and Vassilenko, 1994).

The secondary structure content of cytochrome GSU1740, and the effect of the temperature on it, was studied using Circular Dichroism (CD). The far-UV CD spectrum is indicated in Figure 3.20. In the native state, the spectrum is typical of a folded protein with high α-helix content, featuring intense negative bands at 209 nm and 220 nm (Figure 3.21.(A), solid line), which in accordance with the secondary structure content estimated by the BeStSel webtool (http://bestsel.elte.hu) (Figure 3.21.(B)).

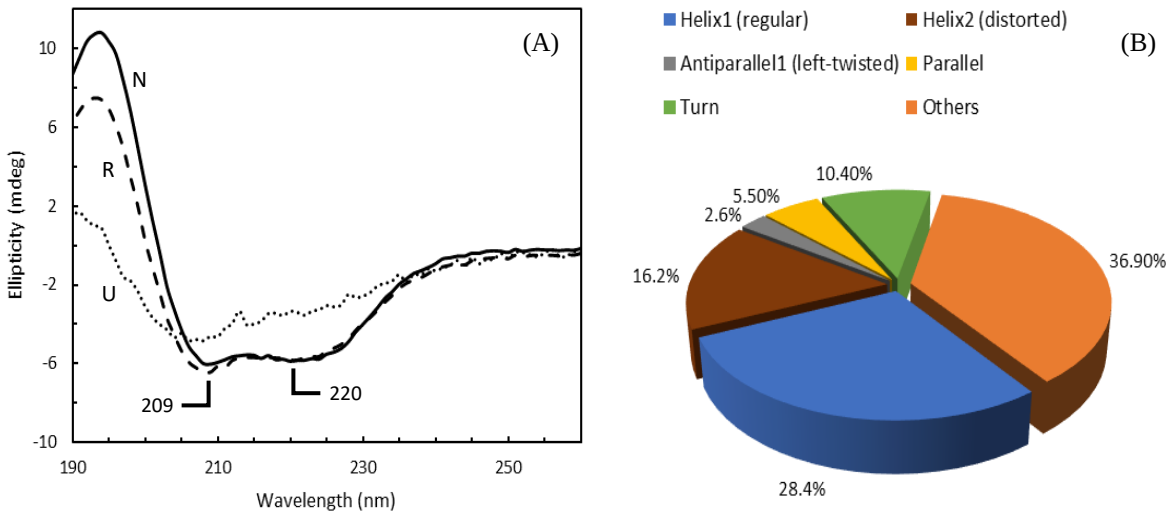

Figure 3.21. (A): Far-UV CD spectra of cytochrome GSU1740 in the native at 25 ºC (N, solid line) and after incubation at 95 ºC (U, dotted line) followed by cooling back to 25 ºC (R, dashed line). (B): Estimated secondary structure content of cytochrome GSU1740 (http://bestsel.elte.hu).

The thermal stability of the protein was also monitored by observing the temperature-induced unfolding at 222 nm (see Figure 3.22). The temperature increasing resulted in a progressive α-helix to random coil transition with loss of the folded spectral features (see Fig. 3.21.(A), dotted line). The melting curve for cytochrome GSU1740, obtained with Boltzmann sigmoidal fitting of the data, does not show a total unfolding of the protein, since the post-transition zone is not defined, therefore it is not possible to estimate the value of midpoint thermal unfolding (Tm) from here (see Figure 3.22). After cooling down the sample back to 25 ºC the original spectrum is obtained (see Figure 3.21.(A)) suggesting that the temperature denaturation is reversible.

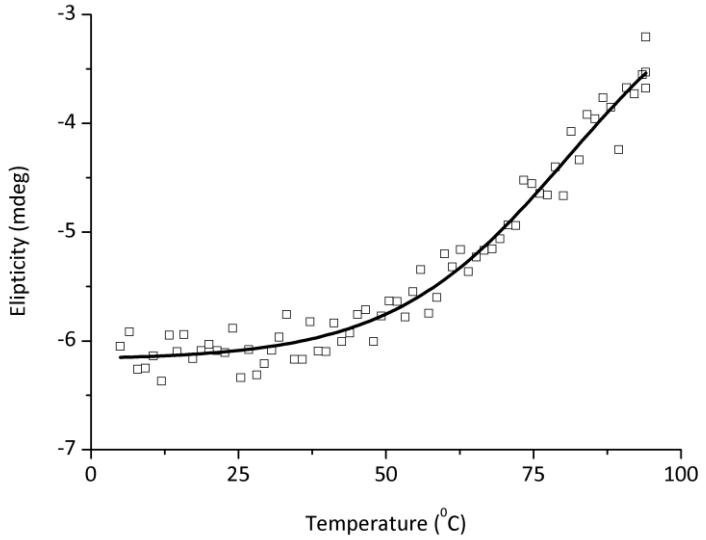

Figure 3.22. Melting curve for cytochrome GSU1740, obtained with Boltzmann sigmoidal fitting of the data registered at λ = 222 nm. Temperature ramp: 5 – 94 ºC (1 ºC/min).

3.6. Electrochemical studies

Instead of measuring the electrochemical response associated with a transient and reversible adsorption process, in which the electrode surface acts similarly to an enzyme turning-over a substrate, it is possible to immobilize proteins, often irreversibly, on the electrode surface. The proteins usually maintain their native function after immobilization on the PG [14,15,16]. Immobilization also removes macromolecular diffusion from electrochemical measurements, greatly simplifying the interpretation of protein voltammetry data and allowing analyses to be carried out with small amounts of protein sample [17,18].

The thin layer theory is applied when all the electroactive species are confined to a thin layer at the electrode surface. If the thickness of this layer is smaller than the diffusion layer (small volume), electrolyse can be fast and complete because each reactant particle has immediate access to the electrode surface, and the diffusion-controlled mass transfer can generally be voided (high sensitivity). Surface-active impurities are virtually excluded from the electrode surface unless they are present at high concentrations. Thin-layer electrodes employ lower direct-current densities than for conventional electrodes, making them more sensitive and well suited for the study of slow electrode reactions [19].

The voltammograms obtained for cytochrome GSU1740 at room temperature (25 ºC) and pH 6, 7 or 8, obtained at different scan rates are presented in Figure 3.23. For each experiment, cyclic voltammograms were recorder at different scan rates, from 2.5 to 20 mV·s^{-1}.

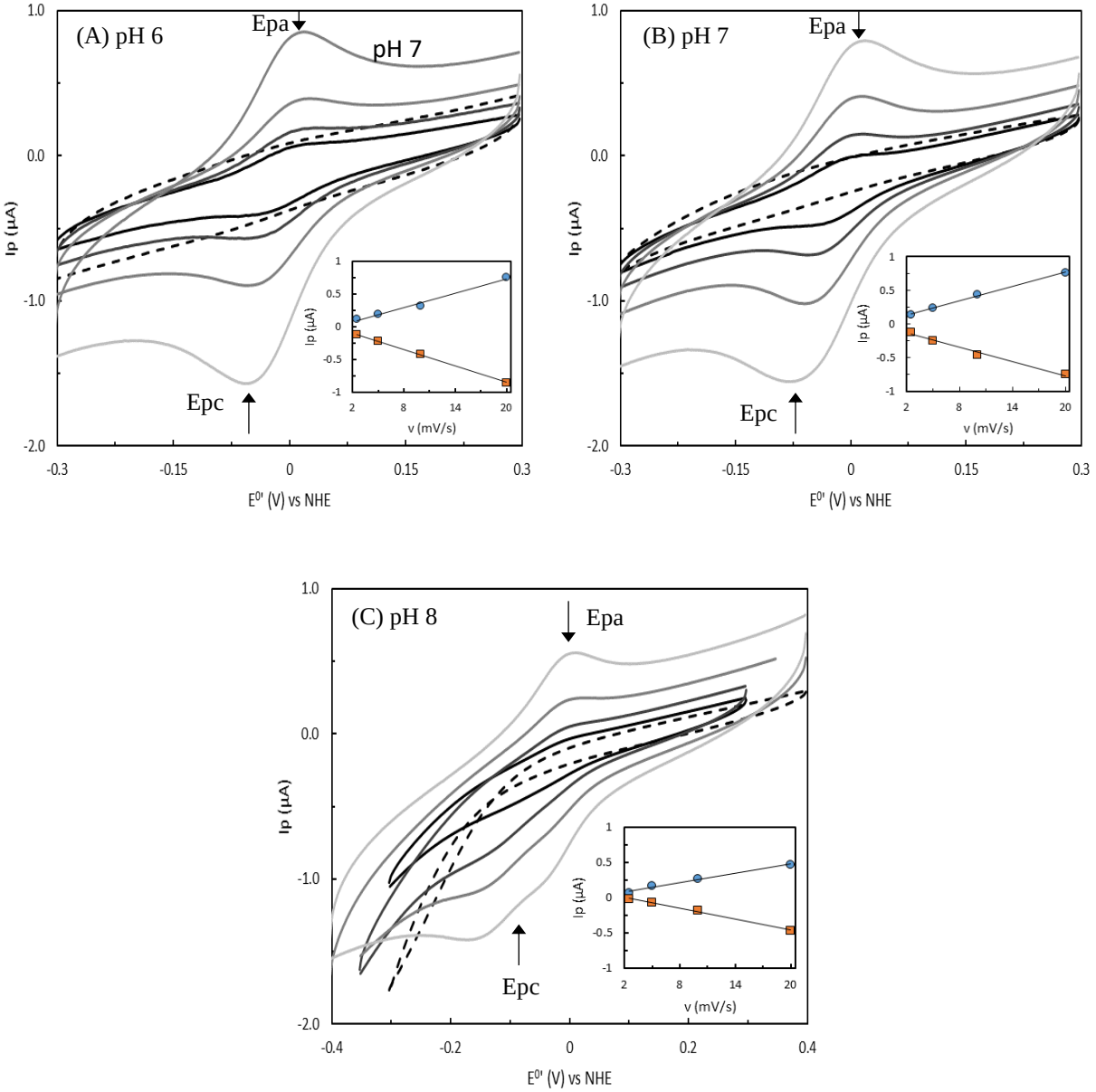

Figure 3.23. (A): Cyclic voltammograms of cytochrome GSU1740 at scan rates (ν) from 2.5 to 20 mV·s^{-1}, at pH 6; the dashed line represents the control at 10 mV·s^{-1}. (B): Cyclic voltammograms of cytochrome GSU1740 at scan rates (ν) from 2.5 to 20 mV·s^{-1}, at pH 7; the dashed line represents the control at 10 mV·s^{-1}. (C): Cyclic voltammograms of cytochrome GSU1740 at scan rates (ν) from 2.5 to 20 mV·s^{-1}, at pH 8; the dashed line represents the control at 20 mV·s^{-1}. All the experiments were performed at room temperature (25 ºC). All the controls, in the absence of protein, were prepared in the same experimental conditions. All insets: peak current as a function of the scan rate, with anodic and cathodic peak currents represented by squares and circles, respectively. Epa and Epc correspond to the anodic and cathodic peaks, respectively.

In agreement with the single redox centre predicted for GSU1740, the cyclic voltammograms obtained show that the protein has one redox pair. In fact, at pH 6 and 7 only a cathodic and anodic peak are observable. At pH 8 two cathodic peak are observable probably due to conformational changes. From the analysis of the voltammograms it was possible to obtain the redox potential values at each pH (Table 3.1). The formal redox potentials (E^0) were calculated according to Equation 3.1, where Epa and Epc correspond to the anodic and cathodic potentials of the respective peaks. The obtained redox potential values were then corrected for the NHE reference scale using Equation 3.2, taking into consideration the experimental temperature dependence of the reference electrode [20, 21, 22].

$$E^0 \text{ vs Ag (V)} = (E_{pa} + E_{pc}) / 2 \quad (3.1)$$

$$E^0 \text{ vs NHE (V)} = 197 - 1.01 \times (T - 25\ ^0C) \quad (3.2)$$

Table 3.1. Redox potential values obtained for cytochrome GSU1740 at room temperature (25 ºC) and pH 6, 7 or 8.

pH	E^0 (mV) vs NHE
6	- 14.3 ± 3.3
7	- 21.5 ± 3.0
8	-66.8 ± 11.8

The data obtained showed that the redox potential of the heme group is affected by the pH (redox-Bohr) effect, indicating that this parameter is modulated by the level of protonation of a neighbouring acid-base group. The identification of this group will only be possible when detailed structural data is obtained.

3.7. References

[1] L. Thöny-Meyer, Biogenesis of Respiratory Cytochromes in Bacteria, Microbiol. Mol. Biol. Rev., 61 (1997) 337–376.

[2] L. Thöny-Meyer, F. Fischer, P. Künzler, D. Ritz, H. Hennecke, *Escherichia coli* Genes Required for Cytochrome *c* Maturation, J. Bacteriol., 177 (1995) 4321–4326.

[3] J.M. Dantas, D.M. Tomaz, L. Morgado, C.A. Salgueiro, Functional characterization of PccH, a key cytochrome for electron transfer from electrodes to the bacterium *Geobacter sulfurreducens*, FEBS Lett., 587 (2013) 2662–2668.

[4] G.R. Moore, G.W. Pettigrew, Cytochromes *c*: Evolutionary, Structural and Physicochemical Aspects, Springer-Verlag Berlin Heidelberg, 1990.

[5] P.R. Pokkuluri, M. Pessanha, Y.Y. Londer, S.J. Wood, N.E.C. Duke, R. Wilton, T. Catarino, C.A. Salgueiro, M. Schiffer, Structures and Solution Properties of Two Novel Periplasmic Sensor Domains with c-Type Heme from Chemotaxis Proteins of *Geobacter sulfurreducens*: Implications for Signal Transduction, J. Mol. Biol., 377 (2008) 1498–1517.

[6] T. Catarino, M. Pessanha, A.G. De Candia, Z. Gouveia, A.P. Fernandes, P.R. Pokkuluri, D. Murgida, M.A. Marti, S. Todorovic, C.A. Salgueiro, Probing the Chemotaxis Periplasmic Sensor Domains from *Geobacter sulfurreducens* by Combined Resonance Raman and Molecular Dynamic Approaches: NO and CO Sensing, J. Phys. Chem. B, 114 (2010) 11251–11260.

[7] H. Theorell, Å. Åkesson, Studies on Cytochrome *c*. I. Electrophoretic Purification of Cytochrome *c* and its Amino Acid Composition, J. Am. Chem. Soc., 63 (1941) 1804–1811.

[8] H. Theorell, Å. Åkesson, Studies on Cytochrome *c*. II. The Optical Properties of Pure Cytochrome *c* and Some of Its Derivatives, J. Am. Chem. Soc., 63 (1941) 1812–1818.

[9] G.W. Pettigrew, G.R. Moore, Cytochromes *c*: Biological Aspects, Springer-Verlag Berlin Heidelberg, 1987.

[10] A. Schejter, P. George, The 695-mμ Band of Ferricytochrome *c* and Its Relationship to Protein Conformation, Biochemistry, 3 (1964) 1045–1049.

[11] E. Shechter, P. Saludjian, Conformation of ferricytochrome c IV Relationship between optical absorption and protein conformation, Biopolymers, 5 (1967) 788–790.

[12] I. Moura, M.Y. Liu, C. Costa, M.C. Liu, G. Pai, A.V. Xavier, J. LeGALL, W.J. Payne, J.J.G. Moura, Spectroscopic characterization of a high-potential monohaem cytochrome from *Wolinella succinogenes*, a nitrate-respiring organism, Redox and spin equilibria studies, Eur. J. Biochem., 177 (1988) 673–682.

[13] G.D. Fasman, Circular Dichroism and the Conformational Analysis of Biomolecules, Springer Science+ Business Media, New York, MA, 1996.

[14] H. Allen, O. Hill, Bio-electrochemistry, Pure & Appl. Chem., 59 (1987) 743–748.

[15] C.F. Blanford, The birth of protein electrochemistry, Chem. Commun., 49 (2013) 11130–11132.

[16] C.F. Blanford, F.A. Armstrong, The pyrolytic graphite surface as an enzyme substrate: microscopic and spectroscopic studies, J. Solid State Electrochem., 10 (2006) 826–832.

[17] C. Léger, S.J. Elliott, K.R. Hoke, L.J.C. Jeuken, A.K. Jones, F.A. Armstrong, Enzyme Electrokinetics: Using Protein Film Voltammetry To Investigate Redox Enzymes and Their Mechanisms, Biochemistry, 42 (2003) 8653–8662.

[18] C. Léger, P. Bertrand, Direct Electrochemistry of Redox Enzymes as a Tool for Mechanistic Studies, Chem. Rev., 108 (2008) 2379–2438.

[19] A.T. Hubbard, D.G. Peters, Electrochemistry in Thin Layers of Solution, C R C Crit. Rev. Anal. Chem., 3 (1973) 201–242.

[20] D.T. Sawyer, A. Sobkowiak, J.L. Roberts Jr., Electrochemistry for Chemists, 2. ed, John Wiley & Sons, Inc., New York, 1995.

[21] A. Lindgren, T. Larsson, T. Ruzgas, L. Gorton, Direct electron transfer between the heme of cellobiose dehydrogenase and thiol modified gold electrodes, J. Electroanal. Chem., 494 (2000) 105–113.

[22] Y. Liu, L.C. Seefeldt, V.D. Parker, Entropies of Redox Reactions between Proteins and Mediators: The Temperature Dependence of Reversible Electrode Potentials in Aqueous Buffers, Anal. Biochem., 250 (1997) 196–202.

4. CONCLUSIONS AND FUTURE PERSPECTIVES

The work developed in this Dissertation contributed to the biochemical characterization of a cytochrome GSU170 a key protein for the respiratory electron transfer pathways from *G. sulfurreducens*. The DNA sequence of the gene encoding to the cytochrome was cloned using a pVA203-PpcC plasmid, a pUC derivative containing an ampicillin resistance gene, a *lac* promoter, which allows for the induction of transcription in the presence of IPTG and an *OmpA leader* sequence. The expression and purification protocols were optimized for the production of the cytochrome yielding approximately 4 mg of protein per litre of cell (*E. coli* BL21 – DE) culture. The data obtained from the different biochemical methods used showed that cytochrome GSU1740 contains one heme group axially coordinated by one histidine and one methionine residue. The dominant secondary elements of the protein are α-helices, as determined by CD spectroscopy. The complementary UV-visible absorption and NMR studies also suggest that the heme is high spin and low spin in the oxidized and reduced state, respectively. The redox potential of the cytochrome (- 21.5 mV) is relatively low compared with the majority of the His-Met cytochromes described in the literature that show typically more positive redox potential values.

Thus, future studies should mainly focus on the structural characterization of this cytochrome. Given the heme spin character in the oxidized state (high spin) the solution structure should be pursued in the reduced form (low spin). In order to do this it is necessary to isotopically label ($^{13}C/^{15}N$) to assist the assignment of the protein signals and thus the structure calculation. Preliminary assays were carried out on this Dissertation, which suggested that the protein is not expressed in the standard conditions described for the isotopic labelling of *c*-type multiheme cytochromes overexpressed in *E. coli* (A.P. Fernandes et al. 2008). Supplementation of the minimal media with glycerol could be one of the solutions. Once the assignment of the NMR signals of protein is established it can be further explored, to identify the interacting regions between these proteins and its redox partners. Meanwhile, it will be important to identify the distal axial heme ligand. The analysis of the cytochrome's sequence indicates three possible candidates: M92; M96 and H98. During the time course of this Dissertation these residues were replaced by alanine residues and vectors containing each mutation were also obtained.

5. APPENDICES

Appendix 1. Composition of solutions used in experimental procedures

Table 5.1. List of the reagents used in this Dissertation. The name of the reagents and their respective concentration and supplier are indicated.

Solutions		Composition
2xYT liquid medium		16 g/L Tryptone (VWR Chemicals) (w/v)
		10 g/L Yeast extract (NZYTech) (w/v)
		5 g/L Sodium chloride (NaCl) (NZYTech) (w/v)
2xYT solid medium		16 g/L Tryptone (VWR Chemicals) (w/v)
		10 g/L Yeast extract (NZYTech) (w/v)
		5 g/L NaCl (NZYTech) (w/v)
		15 g/L Bacteriological agar (VWR Chemicals) (w/v)
LB liquid medium		10 g/L tryptone (VWR Chemicals) (w/v)
		5 g/L yeast extract (NZYTech) (w/v)
		10 g/L Sodium chloride (NaCl) (NZYTech) (w/v)
LB solid medium		10 g/L tryptone (VWR Chemicals) (w/v)
		5 g/L yeast extract (NZYTech) (w/v)
		10 g/L Sodium chloride (NaCl) (NZYTech) (w/v)
		15 g/L Bacteriological agar (VWR Chemicals) (w/v)
Lysis buffer		100 mM Tris-HCl buffer pH 8.0
		0.5 mM EDTA (Sigma-Aldrich)
		20 % sucrose (Fisher Scientific) (w/v)
Loading buffer		4 % SDS (w/v)
		11.5 % glycerol (v/v)
		125 mM Tris-HCl buffer pH 6.8
		0.2 % azul de bromofenol (w/v)
Heme staining solutions	A	15 mg TMBZ (Acros Organics)
for SDS-PAGE		15 mL methanol 100 % (Fisher Chemical)
	B	0.25 M Sodium acetate buffer pH 5
	C	15 mL solution A
		35 mL solution B
	D	35 mL solution B
		15 mL propanol (VWR Chemicals)
Sodium acetate buffers		Sodium acetate trihydrate (Scharlau)
		Acetic acid 99.8 % (Sigma-Aldrich)
Tris-HCl buffers		Tris base (NZYTech)
		Hydrochloric acid 37 % (Carlo Erba)

Appendix 2. Experimental Protocols

Appendix 2A. SDS-PAGE gel electrophoresis

Throughout the work presented in this Dissertation, the protein purity was repeatedly evaluated by SDS-PAGE, using a Mini-Protean® Electrophoresis System (Bio-Rad). The SDS-PAGE gel recipe (5% stacking gel and 15% running gel) is presented in the table below.

Table 5.2. SDS-PAGE gel recipe for 5% stacking gel and 15% running gel.

Stock solutions	Stacking gel (µL)	Running gel (µL)
1.5 M Tris-HCl pH 8.8	--	750
0.5 M Tris-HCl pH 6.8	450	--
40 % acrylamide/bis-acrylamide (37.5:1)	225	1880
10 % SDS	18	50
H_2O	1107	2280
10 % PSA	13.5	38
TEMED	2	2.5

The same loading buffer (2 % SDS, 5 % glycerol, 0.01 % bromophenol blue, in 62.5 mM Tris-HCl pH 6.8) was used for all the samples, which were loaded after an incubation time of 5 minutes at 95 ºC. The electrophoresis were run in 1x SDS running buffer (25 mM Tris, 192 mM glycine, 1% SDS), at 120 V for 70 minutes. The molecular weight marker used was the Precision Plus ProteinTM Dual Xtra Standards (Bio-Rad) (see Figure 5.1).

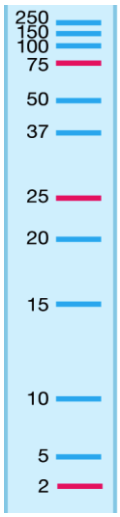

Figure 5.1. Protein molecular weight marker *Precision Plus Protein™ Dual Xtra Prestained Protein Standards* (Bio-Rad). The numbers on the left refer to the molecular weight of each band, in kDa.

Appendix 2B. Staining of SDS-PAGE gel electrophoresis

Heme proteins can be detected using TMBZ as a chromogenic electron donor and H_2O_2 as an electron acceptor, which gives rise to light blue bands.

First, the gel was transferred to the solution C (composition in Appendix 1), containing TMBZ (Acros Organics), and left sheltered from light for 30 minutes. After that, 300 μL of H_2O_2 30 % (w/w) (Sigma-Aldrich) were added, followed by 30 min of gentle shaking. Finally, the gel was washed twice with the solution D (composition in Appendix 1).

The heme staining of SDS-PAGE electrophoresis gels is based on the peroxidase activity of the heme group. The heme group of any cytochrome is capable of using H2O2 has an electron acceptor and catalyse an oxidative reaction until the formation of H2O. Based on this, in the heme staining of SDS-PAGE gels, tetramethylbenzidine (TMBZ, from Acros Organics) is used as a chromogenic electron donor (TMBZ forms a blue precipitate when oxidized, leading to light blue bands in the SDS-PAGE gel) and H2O2 as an electron acceptor. In order for this staining technique to work, the heme(s) group(s) have to be in the oxidized state and so, the loading-buffer used does not contain β-mercaptoethanol.

After running the SDS-PAGE electrophoresis, the gel is placed in a solution containing TMBZ (Solution C) for 30 minutes. The gel must be incubated while stirring with no light exposure. Then, 300 μL of 30 % H_2O_2 are directly added, followed by another 30 minutes of incubation. Finally, the gel is washed twice with a sodium acetate/propanol solution (Solution D). The necessary solutions for this staining method are indicated in the table of Appendix 1.

BlueSafe is a protein stain which consists of a safer alternative to the traditional Coomassie Blue staining for detecting proteins because it doesn't contain any methanol or acetic acid in its composition and doesn't require the use of a distaining solution.

Appendix 2C. Agarose gel electrophoresis

Throughout the work presented in this Dissertation, the purity of the PCR products was evaluated by agarose gel electrophoresis, using a kuroGel Midi 13 Horizontal Electrophoresis System (VWR). The agarose gels were prepared by adding either 1 or 1.3 g of agarose (for 1 and 1.3 % agarose gels, respectively) to 100 mL of 1x TAE buffer (40 mM Tris, 20 mM acetic acid and 1 mM EDTA) and 1 µL of GreenSafe Premium (NZYTech).

GreenSafe Premium is a new nucleic acid stain, introduced by NZYTech, that can be used as a safer alternative to the traditional ethidium bromide for detecting nuclei acids in agarose gels. It is as sensitive as ethidium bromide and can be used exactly in the same way in agarose gel electrophoresis. This stain emits green fluorescence when bound to DNA or RNA, having two secondary fluorescence excitation peaks (around 270 and 290 nm) and one strong excitation peak centred at 530 nm.

All the samples were loaded with the same loading buffer (1x DNA gel loading dye, from Fermentas). The electrophoresis were run in 1x TAE running buffer, at 90 V for 60 minutes. The DNA ladder used was the 1 kb DNA ladder, from New England Biolabs (Figure 5.2).

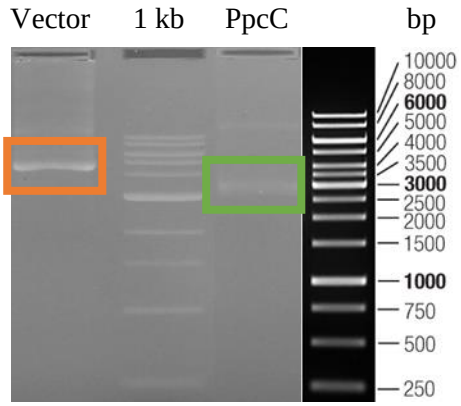

Figure 5.2. Resulting product (Vector) of the second PCR cycle, analysed by 1.5 % agarose gel electrophoresis, stained with GreenSafe Premium (NZYTech) and observed under UV light (VWR UV transilluminator). PpcC: pVA203-PpcC plasmid. 1kb: *Thermo Scientific™ GeneRuler™* 1kb DNA Ladder from New England Biolabs. The numbers on the right refer to the number of base-pairs of each band.